Evaluation of SO_2, SO_4^{2-} and an updated SO_2 dry deposition parameterization in UKESM1

Catherine Hardacre[1], Jane P. Mulcahy[1], Richard Pope[2,3], Colin G. Jones[3], Steven T. Rumbold[3], Can Li[4,5], Colin Johnson[3], and Steven T. Turnock[1,6]

[1]Met Office, Exeter, EX1 3PB, UK
[2]School Earth and Environment, University of Leeds, Leeds, UK
[3]National Centre for Atmospheric Science, University of Leeds, Leeds, UK
[4]NASA Goddard Space Flight Center, Greenbelt, MD 20771, USA
[5]Earth System Science Interdisciplinary Center, University of Maryland, College Park, MD 20742, USA
[6]University of Leeds Met Office Strategic (LUMOS) Research Group, School of Earth and Environment, University of Leeds, UK

Correspondence: Catherine Hardacre (catherine.hardacre@metoffice.gov.uk)

Abstract. In this study we evaluate simulated surface SO_2 and sulphate (SO_4^{2-}) concentrations from the United Kingdom Earth System Model (UKESM1) against observations from ground based measurement networks in the USA and Europe for the period 1987 to 2014. We find that UKESM1 captures the historical trend for decreasing concentrations of atmospheric SO_2 and SO_4^{2-} in both Europe and the USA over the period 1987 to 2014. However, in the polluted regions of the eastern

5   USA and Europe, UKESM1 over-predicts surface SO_2 concentrations by a factor of 3, while under-predicting surface SO_4^{2-} concentrations by 25-35%. In the cleaner western USA, the model over-predicts both surface SO_2 and SO_4^{2-} concentrations by a factor of 12 and 1.5 respectively. We find that UKESM1's bias in surface SO_2 and SO_4^{2-} concentrations is variable according to region and season. We also evaluate UKESM1 against total column SO_2 from the Ozone Monitoring Instrument (OMI) using an updated data product. This comparison provides information about the model's global performance, finding

10 that UKESM1 over predicts total column SO_2 over much of the globe, including the large source regions of India, China, the USA and Europe as well as over outflow regions. Finally, we assess the impact of a more realistic treatment of the model's SO_2 dry deposition parameterization. This change increases SO_2 dry deposition to the land and ocean surfaces, thus reducing the atmospheric loading of SO_2 and SO_4^{2-}. In comparison with the ground-based and satellite observations, we find that the modified parameterization reduces the model's over prediction of surface SO_2 concentrations and total column SO_2. Relative

15 to the ground-based observations the simulated surface SO_4^{2-} concentrations are also reduced, while the simulated SO_2 dry deposition fluxes increase.

Copyright statement. TEXT

1 Introduction

Anthropogenic sulphur dioxide (SO_2) emissions have been the main driver of the historical aerosol effective radiative forcing (ERF) since the mid 20th century (Boucher et al., 2013). SO_2 is emitted into the atmosphere from a number of anthropogenic (and natural) sources and once in the atmosphere SO_2 can be oxidised to form sulphate (SO_4^{2-}) aerosol, which plays a key role in both acid deposition, atmospheric aerosol loading and cloud properties, thereby directly influencing the Earth's radiative balance. For Earth system models (ESMs) to have a good representation of the historical climate and thereby give us confidence in their future projections, it is extremely important that they can capture the sulphur cycle. The UK's Earth system model (UKESM1), in common with other ESMs, has a cold bias in the mid 20th century which looks to be associated with an excessively negative aerosol ERF (Sellar et al., 2019; Seland et al., 2020). A key component of the analysis and development of UKESM1 focuses on the model's sulphur cycle and its link to historical aerosol forcing. Mulcahy et al. (2020) conducted an in-depth evaluation of the aerosol species in UKESM1 and its physical model component, HadGEM3-GC3.1, including SO_4^{2-} and uncovered some interesting differences in the sulphur budget between these two models including differences in the SO_2 lifetimes and oxidant loading. We aim to extend their work by conducting a detailed evaluation of SO_2 and by probing deeper into the process level uncertainty of the sulphur cycle.

Sources of SO_2 include industry, energy, land-based transport, shipping, volcanoes, biomass burning and marine di-methyl sulphide (DMS) (Feng et al., 2020; Fioletov et al., 2016; Liu et al., 2018; Janssens-Maenhout et al., 2015; Crippa et al., 2018). Total global emissions of SO_2 increased to a peak value of approximately $180\,\mathrm{Tg}$ SOx (as SO_2) y^{-1} in the 1970s, but following emission reduction policies to improve air quality and reduce acid deposition that were implemented in the 1980s (Hoesly et al., 2018), total global emissions had decreased to approximately $120\,\mathrm{Tg}$ SOx y^{-1} by 2015 (Aas et al., 2019). This trend is captured in global models, but there is substantial temporal variation at the regional scale (Aas et al., 2019). Legislation has driven reductions in SO_2 emissions and subsequently SO_4^{2-} aerosol across Europe (Torseth et al., 2012) and North America (Sickles II and Shadwick, 2015; Holland et al., 1998). In these regions reductions in SO_2 emissions have had important environmental and health benefits as well as climate impacts. Turnock et al. (2015) found that between 1970 and 2010 surface SO_4^{2-} aerosol reduced by about 70% in the observations and also in the simulations. For the same period, top of atmosphere (TOA) aerosol radiative forcing over this region increased by $>3\,\mathrm{W}\,m^{-2}$ in response to these changes in anthropogenic emissions. Similarly Leibensperger et al. (2012) reported that over the USA aerosol ~~raditive~~ radiative forcing decreased by $1.0\,\mathrm{W}\,m^{-2}$ in the period from 1990 to 2010. Emission reduction policies in China have been implemented since 2013, which has reduced anthropogenic SO_2 emissions (Aas et al., 2019; Zheng et al., 2018; Hoesly et al., 2018; Liu et al., 2018; Krotkov et al., 2016), and subsequently driven decreases in aerosol optical depth (AOD) (Zhao et al., 2017). However, SO_2 emissions from India continue to increase (Aas et al., 2019; Liu et al., 2018; Krotkov et al., 2016).

Good representation of the sulphur cycle in models is essential for constraining uncertainties associated with the impacts of aerosols on the Earth system and thus understanding the global climate. The global atmospheric loading of SO_2 is controlled

by the emissions (sources) to the atmosphere and the loss processes, which are oxidation to SO_4^{2-}, dry deposition and wet deposition. Global scale SO_2 emissions are represented in ESMs using emission inventories such as HTAP (Janssens-Maenhout et al., 2015), OMI-HTAP (Liu et al., 2018), EDGAR (Crippa et al., 2018) and CMIP6 (Feng et al., 2020), the latter being

55   developed for use by models participating in the CMIP6 project (Eyring et al., 2016). Although uncertainty in SO_2 emissions is relatively low (Hoesly et al., 2018), in bottom up inventories such as HTAP and EDGAR there may be uncertainty in the emission and activity factors, in the conversion from country scale to grid scale, and the input data may be incomplete or subject to rapidly changing economic and/or policy conditions (Janssens-Maenhout et al., 2015). In satellite derived data sets there is uncertainty associated with the retrieval methods and the signal to noise ratio, which can make smaller sources and background

60   concentrations more difficult to detect (Fioletov et al., 2016). Yang et al. (2019) have also found that injection height is a larger source of uncertainty in model representation of SO_2 emissions than inventory uncertainty, affecting surface concentrations by $70-130\%$ depending on sector and region, compared with $8-14\%$ from inventory uncertainty. The impact of injection height in UKESM1 was demonstrated by Mulcahy et al. (2020) who found that emitting SO_2 higher in to the atmosphere, rather than in to the lowest model level increased the burden from $0.53\,\mathrm{Tg}$ to $0.61\,\mathrm{Tg}$ and the lifetime from 2.08 to 2.21 days, although

65   SO_4^{2-} was not significantly affected.

Anthropogenic emissions of SO_2 are generally from point sources such as power stations or smelters. Once emitted SO_2 has a lifetime of approximately two days, although this can vary from $15\,\mathrm{h}$ to $65\,\mathrm{h}$ in summer and winter, respectively (Lee et al., 2011). The ~~relatively short~~ lifetime of SO_2 ~~means~~ depends on both wet and dry deposition of the molecule and the oxidation

70   rate to SO_4^{2-}. The ≈ 2 day lifetime is such that much of the loss via oxidation and deposition occurs locally~~, with the ratios of the different loss processes~~. SO_2 loss near sources and the impact of environmental conditions on loss processes have been investigated in a number of studies.

SO_2 deposition is highly dependant on the surface type, soil pH, solar radiation level, near-surface relative humidity and,

75   in particular, whether the underlying surface is wet or dry, with deposition increasing significantly for a wet surface. ~~SO_2 loss near sources and the impact of environmental conditions on these processes have been investigated in a number of studies.~~
Wys et al. (1978) calculated diurnal averaged deposition of emitted SO_2 onto an agricultural field of 35% within $300\,\mathrm{km}$ of the emission source, with daytime deposition significantly higher than at night. The same study found that 15% of emitted SO_2 was dry deposited onto an arid desert surface within $300\,\mathrm{km}$ of the source. Studies over Europe indicate similar rates of deposi-

80   tion and sensitivity to surface type. For example, using flight observations off the East coast of the UK~~Smith and Jeffrey (1975) ., ~~ Smith and Jeffrey (1975) estimated 50% of the SO_2 emitted from UK sources was removed from the atmosphere, or converted to SO_4^{2-} by the time it was observed in air parcels over the North Sea. This amounts to a loss or conversion of 50% emitted SO_2 within ~~≈ 2~~ 200-300 km of the emission source. Smith and Jeffrey (1975) further partitioned this loss into 30-35% due to dry deposition and ~~≈ 2~~ 10-15% oxidation to SO_4^{2-}, with wet deposition making only a minor contribution to

85   the total loss. Similar rates of SO_2 loss have been observed in a number of other observational studies of dry deposition ~~(e.g., Payrissat and Beilke, 1975; ?; Fowler, 1978; Erisman and Baldocchi, 1994)~~(e.g., Payrissat and Beilke, 1975; Garland, 1977; Garland

. Studies analysing SO_2 dispersion around U.S. power stations found that fractional oxidation rates to SO_4^{2-} are sensitive to the amount of solar radiation, with rates ranging from a winter low of $1\times10^{-3}\,h^{-1}$ to a summer high of $1.5\times10^{-2}\,h^{-1}$ (Altshuller, 1979; Meagher et al., 1983). Representing the SO_2 loss processes is challenging for ESMs because $200-300\,km$ is represented by $1-2$ grid cells, meaning that deposition and oxidation are parameterized on the model grid scale and may not capture temporal and spatial variation. In addition there is uncertainty associated with the oxidation and deposition processes.

In the atmosphere SO_2 can be oxidised in the gas phase by hydroxyl (OH) radicals and in the aqueous phase by reactions in cloud and rain water involving hydrogen peroxide (H_2O_2), ozone (O_3), O_2 catalyzed by transition metal ions, and other oxidants, to form SO_4^{2-} ~~, see Turnock et al. (2019) and references within~~(see Turnock et al. (2019) and references within. The oxidation chemistry is necessarily simplified in many models due to the computational cost of detailed chemistry schemes, but studies have shown that oxidant levels can impact the lifetime of aerosol precursor species and ultimately global radiative forcing (Mulcahy et al., 2020; Karset et al., 2018). Uncertainty in aerosol radiative forcing also results from different values of cloud water pH, which alters SO_4^{2-} formation by changing the rate of aqueous phase oxidation of SO_2 by ozone (Turnock et al., 2019). Observations have shown that cloud pH is both temporally and spatially variable (Aleksic et al., 2009; Murray et al., 2013; Schwab et al., 2016; Li et al., 2017), although measurements are very sparse. Typically, this variation is not accounted for in global chemistry climate models, including UKESM1 and its predecessor HadGEM3-GC3.1, both of which use a temporally and spatially constant cloud pH of 5.0. Turnock et al. (2019) found that increasing the cloud pH by 1.0 in HadGEM3-GC3.1 reduced the total SO_2 column by up to 50% over Europe, North America, and East Asia for 1970–1974 and 2005–2009. The impact on SO_4^{2-} was variable due to the different SO_2 loadings over the different regions and in the different time periods. Overall aerosol radiative forcings varied by up to $4\,W\,m^{-2}$, with larger changes in some regions depending on whether cloud water pH was assumed to have increased or decreased over recent decades.

Loss of SO_2 and SO_4^{2-} to the Earth's surface by deposition can be through dry or wet processes. Dry deposition describes the removal of a gas or particle through direct contact of air with the Earth's surface and wet deposition describes the incorporation of gases or particles into rain droplets or snow crystals and their subsequent removal through precipitation. Globally dry deposition removes around 45% of SO_2 from the atmosphere (Chin et al., 2000). The importance of dry deposition in the global sulphur budget is the reason why we target it for ~~improvement~~ development in UKESM1. Dry deposition of SO_2 in ESMs is generally represented by a resistance in series approach (e.g. Archibald et al., 2020; Wu et al., 2020). Deposition of SO_4^{2-} is mainly via wet processes (approximately 90%, Chin et al., 2000), including gravitational settling and rain out. Deposition processes are necessarily parametrized in global models because they occur at sub-grid scales and this contributes to model uncertainty. Further, observational flux data sets are sparse and frequently temporally and spatially limited, hindering model ~~evalaution~~ evaluation of deposition processes at regional to global scales.

~~The main challenge in evaluating model's ability to capture historical trends in sulphur species is the scarcity of observational data. Following the~~ Sulphur species are relatively well observed compared to many atmospheric components as their role in air

pollution is well established. In the 1970's and 1980's the increasingly detrimental impacts of rising SO_2 emissions on acid deposition, air quality and human health in Europe and North America led to monitoring networks being set up in these regions (Torseth et al., 2012; MACTEC-Engineering and Consulting, 2005). Rising pollution in Asia also led to the establishment of the The Acid Deposition Monitoring Network in East Asia (EANET) in 2001 (e.g. Wang et al., 2008). However, even with these data sets it is only possible to evaluate model simulations of the recent historical period and similar data sets are not available for other large source regions such as India, the Middle East, or remote regions. Further, the lack of a range of measurements, including flux observations, hinders detailed process studies at large scales. Since the early 2000's satellite observations of near surface SO_2 have also become available. Of these, the satellite data sets with the best temporal resolution and spatial coverage for SO_2 are from the Ozone Monitoring Instrument aboard the NASA Earth Observing System Aura spacecraft (Fioletov et al., 2016). Although biases in the SO_2 retrieval from OMI limit its use at high and low latitudes in winter and over areas with low atmospheric SO_2 loading, they do provide valuable information over regions where there are no long term, or even any ground-based observations (Li et al., 2020; Levelt et al., 2018).

This paper is configured as follows; the model (UKESM1), the model simulations, observation data sets and modifications to UKESM1's SO_2 dry deposition parameterization are described in Section 2. In Section 3 we evaluate UKESM1 against observations of surface SO_2 and SO_4^{2-} and total column SO_2. In Section 4 we assess the impact of the modifications to UKESM1's SO_2 dry deposition parameterization. The discussion and conclusions are presented in Sections 5 and 6.

2 Methods

2.1 UKESM1

UKESM1 is the latest generation Earth System (ES) model developed in the UK. UKESM1 has HadGEM3-GC3.1 (Kuhlbrodt et al., 2018; Williams et al., 2018) as its physical-dynamical core. HadGEM3-GC3.1 is comprised of the Global Atmosphere 7.1 (GA7.1) configuration of the Unified Model (UM) (Walters et al., 2019; Mulcahy et al., 2018); the Nucleus for European Modelling of the Ocean (NEMO) model (Storkey et al., 2018); the Los Alamos Sea Ice Model (CICE, Ridley et al., 2018) and the Joint UK Land Environment Simulator (JULES) land surface model (Best et al., 2011). The additional ES process models include the stratospheric-tropospheric (StratTrop) version of the United Kingdom Chemistry and Aerosol (UKCA) model (Archibald et al., 2020), the Model of Ecosystem Dynamics, nutrient Utilisation, Sequestration and Acidification, (MEDUSA, Yool et al., 2013) and the terrestrial biogeochemistry component of JULES (Clark et al., 2011). UKESM1 is described in detail, along with its component models and the coupling between them, by Sellar et al. (2019). The aerosol scheme used in UKESM1 (GLOMAP-Mode, Mann et al., 2010), including SO_2 emissions and chemistry, is described in detail by Mulcahy et al. (2020). In UKESM1 the land and atmosphere share a regular latitude–longitude grid with a resolution of $1.25° \times 1.875°$ (approximately 135 km at the mid latitudes). There

are 85 vertical levels on a terrain following hybrid height coordinate with a model lid at 85 km above sea level and 50 of these
levels below 18 km. The ocean has a horizontal resolution of 1° and 75 vertical levels. While the atmospheric time step of the
model physics is 20 minutes, due to the inherent computational cost of the chemistry and aerosol components, both of these
components are called once per hour.

In UKESM1 the SO_2 emissions, including anthropogenic sources are from the CMIP6 inventory (Feng et al., 2020). Large
explosive volcanic sources and biomass burning sources are not interactively modelled, but prescribed using the CMIP6 strato-
spheric aerosol climatology (Sellar et al., 2019) and van Marle et al. (2017) emissions inventory respectively. Continuously
degassing volcanic sources are also included as present-day, three-dimensional, temporally fixed (i.e. no seasonal variation)
fields (Dentener et al., 2006). Emissions from the energy and industrial sectors are all emitted into the first model layer. We
summarize ~~the~~ how loss of SO_2 from the atmosphere via oxidation, wet and dry deposition is modelled here, but for a detailed
description of these processes in UKESM1 the reader is referred to Archibald et al. (2020) and Mulcahy et al. (2020). ~~Gas
phaser and aqueous phase~~ Gas- and aqueous-phase oxidation of SO_2 to SO_4^{2-} is represented by the reactions shown in Table
1 (Pham et al., 1996; Sander et al., 2003; Kreidenweis et al., 2003). Dry deposition of SO_2 is parameterized following the
resistance in series approach originally developed by Wesely (1989) (see Section 2.2.1). Loss via wet deposition is the SO_2
that is scavenged and subsequently converted to SO_4^{2-} in rainwater. It is parameterized as a first-order loss rate, calculated as
a function of UKESM1's three-dimensional convective and large-scale precipitation (Archibald et al., 2020; O'Connor et al.,
2014). Sulphate aerosol is also removed from the atmosphere by dry and wet deposition (Mulcahy et al., 2020). The aerosol
dry deposition and sedimentation are represented by a resistance in series approach similar to that used for gaseous species,
but which also accounts for aerosol size (Mann et al., 2010). Wet deposition is parameterized in UKESM1 by an in-cloud
convective plume scavenging scheme following the approach described by Kipling et al. (2013) and by nucleation scavenging
(Mulcahy et al., 2020).

Table 1. Summary of SO_2 oxidation chemistry in UKEMS1

Gas phase reactions
$SO_2 + OH \rightarrow SO_3 + HO_2$
$SO_2 + O_3 \rightarrow SO_3$
$SO_3 + H_2O \rightarrow H_2SO_4 + H_2O$
Aqueous phase reactions
$HSO_3^- + H_2O_2 \rightarrow SO_4^{2-}$
$HSO_3^- + O_3 \rightarrow SO_4^{2-}$
$SO_3^{2-} + O_3 \rightarrow SO_4^{2-}$

2.2 SO$_2$ dry deposition parameterization

The UKESM1 parameterization of SO$_2$ dry deposition follows that described in Wesely (1989). This scheme uses the widely accepted approach of calculating the flux of a depositing gas as a function of a deposition velocity multiplied by the concentration gradient of the gas between a reference height (z, e.g. the lowest model level) and the receptor surface (Eqn. 1. The deposition velocity is calculated by analogy with electrical resistance and is inversely proportional to three resistances to deposition, representing the three stages of gaseous transport to a receptor surface. These are: (i) aerodynamic resistance (R_a) to gas transport through the near-surface turbulent layer, (ii) viscous resistance to gas transfer across a quasi-laminar layer surrounding the receptor surface (R_b) and (iii) structural resistance to deposition of the receptor surface itself (R_c). For a detailed description of this approach, see Wesely (1989); Erisman and Baldocchi (1994); Zhang et al. (2003). The deposition velocity is calculated for each fractional surface type in a given model grid box, as is a resulting loss rate (flux) of SO$_2$ from the atmosphere. The loss rates to each fractional surface are combined, resulting in the total loss of SO$_2$ from the model atmosphere due to dry deposition. The deposition velocity is given by Equation 2. If the surface is covered by vegetation, R_a is generally calculated at a zero-plane displacement height z = z - d, where d is usually 0.6-0.8 times the vegetation height in metres. The UKESM1 calculation of R_a and R_b follow standard approaches (see Eqn. 3 and 4). The aerodynamic resistance, R_a, is calculated from the wind profile taking into account atmospheric stability and the surface roughness, where $z0$ is the roughness length, ψ is the Businger dimensionless stability function, κ is von Karman's constant, and u$_*$ is the friction velocity. The quasi-laminar sub-layer resistance, R_b, is calculated with Sc the Schmidt number, and Pr the Prandtl number.

$$F = V_d \times C$$

$$V_d = \frac{1}{R_a + R_b + R_c}$$

The surface or canopy resistance to deposition, R_c, is the most difficult of the three resistances to parameterize as it is sensitive to biochemical details of the individual receptor surfaces. R_c is typically a function of the following receptor-specific resistances: (i) canopy stomatal resistance (R_{stom}) combined with the mesophyll resistance (R_m) of a given plant, (ii) canopy cuticle or external leaf resistance (R_{cut}) and (iii) soil resistance (R_{soil}), combined with an in-canopy resistance (R_{inc}), describing the turbulent transport of a gas through the plant foliage to the ground. The stomatal resistance, leaf cuticle resistance and soil resistance are assumed to operate in parallel. For surfaces not covered with vegetation (e.g. open water, bare soil or snow covered surfaces), R_c is made equal to one of; R_{water}, R_{soil}, R_{snow}. The receptor-specific resistances are combined as shown in Equation 5 to calculate R_c. In UKESM1, R_{stom} follows the approach outlined in Wesely (1989), based on the original work

180

185

190

195

200

205

210

of Baldocchi et al. (1987). R_{stom} is first calculated for water vapour for each vegetation type, R_{stom} for other gases is then derived by scaling R_{stom} for water vapour by the ratio of the diffusion coefficient for the gas in question and that of water vapour. Due to a general lack of knowledge R_m values are assumed to be zero for all gases. In UKESM1 R_{inc} and R_{soil} are combined into a single value (referred to hereafter as R_{soil}). In UKESM1, R_c for SO$_2$ for the 13 fractional land cover types is

215   initially set to the standard surface resistance (R_{surf}) values given in Table A2.

$$F = V_d \times C \tag{1}$$

$$V_d = \frac{1}{R_a + R_b + R_c} \tag{2}$$

220

$$R_a = (ln(\frac{z}{z0}) - \psi)/(\kappa u_*) \tag{3}$$

$$R_b = (Sc/Pr)^{\frac{2}{3}}/(\kappa u_*) \tag{4}$$

225    $$R_c = [\frac{1}{R_{stom} + R_m} + \frac{1}{R_{inc} + R_{soil}} + \frac{1}{R_{cut}}] - 1 \tag{5}$$

2.2.1 Modifications to UKESM1's SO$_2$ dry deposition parameterization

In this study we investigate two changes to the SO$_2$ dry deposition parameterization in UKESM1. Firstly, we account for a key omission in ~~the~~ UKESM1 ~~calculation of~~ in that for R_{cut} and R_{soil} ~~in that~~ no account is taken as to whether the receptor surface is wet or dry, nor of the near surface relative humidity~~or soil pH~~. Observational studies suggest that SO$_2$ dry deposition (through

230   a decrease in R_c) is significantly more efficient over wet surfaces compared to dry surfaces, as well as for increasing values of near surface relative humidity ~~(e.g., ?Fowler, 1978; Erisman and Baldocchi, 1994)~~ due to the high solubility of SO$_2$ in water ~~.~~ ~~Based on these findings we~~ (e.g., Garland and Branson, 1977; Fowler, 1978; Erisman and Baldocchi, 1994; Erisman et al., 1994) . We apply the findings from these studies to extend the calculation of R_{cut} for SO$_2$ in UKESM1 to be a function both of whether the model vegetation is wet or dry and to the near surface relative humidity. This change allows a surface to remain wet

235   after rainfall for a period of three hours, where previously it would have been "dry" immediately after the rainfall event. R_{soil} for SO$_2$ is also made a function of near surface relative humidity. These changes are referred to as ~~R$_{surf}$~~**R$_{surf}$-mod** and will impact SO$_2$ dry deposition over land surfaces. ~~Our approach closely follows that of Erisman and Baldocchi (1994); Erisman et al. (1994) and interested readers are referred to those two articles for more detail~~ We include a more detailed description of the modifications

8

to UKESM1's SO_2 parameterization in Appendix A. Secondly, we change the the surface resistance term for SO_2 dry depo-
sition to water (R_{water}) from an erroneously high value of $148\,s\,m^{-1}$ to $1\,s\,m^{-1}$ to better reflect the high solubility of SO_2 in
water. While lower than the value of $20\,s\,m^{-1}$ used by Zhang et al. (2003), it reflects the small, observed value of $0.004\,s\,m^{-1}$
from ~~?~~Garland (1977). This change is referred to as ~~R_{water}~~**R_{water}-mod** and will impact SO_2 dry deposition predominantly over
the ocean.

In addition to the primary changes to the SO_2 dry deposition parameterization (~~R_{water}~~**R_{water}-mod** and ~~R_{surf}~~**R_{surf}-mod**), we
also include two secondary modifications. These are (1) an update in the calculation of the stability parameter (*z/L*) to better
describe dry deposition in very stable atmospheric conditions, and (2) a bug fix in the dimethyl ~~sulphoxide (DMSO~~sulphide
(DMS) chemistry. The stability parameter (*z/L*) describes the flux profile relationship and is important for calculating ~~the R_a
in Eqn. ??. Here it is updated from the calculation~~ R_a in Equation 3. Here we update the calculation from that given by Dyer
(1974) to that described by Holtslag and Bruin (01 Jun. 1988). We also reduce the reference height for dry deposition (*z*)
from $50\,m$ to $10\,m$ in line with Holtslag and Bruin (01 Jun. 1988). The reference height is the height below which there is no
turbulence in very stable conditions and is also important for calculating ~~R_a~~R_a. The changes to *z/L* and *z* act to reduce the rate
at which the deposition velocity decreases in very stable conditions. The DMSO bug fix corrects the equation for dimethyl
sulphide (DMS) oxidation by OH (see Reaction R1) in UKCA's StratTrop mechanism, where the products incorrectly contain
more sulphur atoms than the reactants. We substitute Reaction R1 with Reactions R2 and R3. This reduces the SO_2 yield to a
maximum of 0.84, which may be further reduced as DMSO deposits to the Earth's surface. However, the changes in simulated
SO_2 are actually only of the order of 1% ~~as~~ because anthropogenic sources are not affected by this change. Although the
secondary changes incorporate important updates in to the model, their impact on the atmospheric SO_2 loading in UKESM1
is small in comparison to that driven by ~~R_{water}~~**R_{water}-mod** and ~~R_{surf}~~**R_{surf}-mod** and we do not discuss it here.

$$C_2H_6S + OH \rightarrow SO_2 + CH_3SO_2OH \tag{R1}$$

$$C_2H_6S + OH \rightarrow 0.6SO_2 + 0.4C_2H_6SO_2 + CH_3O_2 \tag{R2}$$

$$C_2H_6SO_2 + OH \rightarrow 0.6SO_2 + 0.4CH_3SO_2OH. \tag{R3}$$

2.3 Model simulations

For this evaluation we initially use 4 simulations from the 19 member ensemble of historical simulations that were conducted
for UKESM1's contribution to CMIP6 (Sellar et al., 2019; Tang, 2019). The historical simulations cover the period from 1850

to the end of 2014, thus modelling the evolution of climate and composition since the pre-industrial era. These simulations
are forced by transient external forcings of solar variability, land use, well-mixed greenhouse gases and other trace gas emissions and aerosols. The volcanic forcing due to the stratospheric injection of SO_2 from volcanic eruptions is prescribed as a zonal mean climatology of the stratospheric aerosol optical properties over the historical period. All forcings and how they are implemented in UKESM1 are described fully in Sellar et al. (2019). Each historical ensemble member was initialised from a different date in the pre-industrial control simulation (Yool et al., 2020). We use monthly mean output for surface SO_2 and SO_4^{2-} concentrations, and SO_2 dry deposition flux. We use a second four member ensemble of historical simulations to evaluate the impact of the changes to the SO_2 dry deposition parameterization described in Section 2.2.1, hereafter this ensemble is referred to as UKESM1-SO2. The UKESM1-SO2 historical simulations are set up and run as for the UKESM1 historical simulations. To calculate the detailed SO_2 budget we utilise the atmosphere-only configuration of UKESM1 and UKESM1-SO2. This is referred to as the Atmospheric Model Intercomparison Project (AMIP) configuration and allows us to generate the diagnostics required for the budget analysis that were not output in the historical simulations at a reduced computational cost. The UKESM1 AMIP configuration is driven by observed sea surface temperature (SST) and sea ice. It does not include the additional dynamic ocean and land surface components (Eyring et al., 2016). Instead, the required vegetation (vegetation fractions, leaf area index, canopy height) and surface ocean biology fields (DMS and chlorophyll) are taken from a single UKESM1 historical member and are prescribed as ancillary data, thereby maintaining traceability to the fully coupled model. For the SO_2 budget calculations AMIP simulations were run from 1979 to the end of 1983.

Table 2. Summary of model configurations used in this study

	UKESM1	UKESM1-SO2
~~Simulation~~ Configuration	Historical	Historical
No. of members	4	4
Modifications	-	(1) R_{water}-mod and R_{surf}-mod
		(2) Update to z/L and $z = 10\,m$
		(3) DMSO chemistry bug fix
Configuration	AMIP	AMIP
No. of members	1	1
Modifications	-	(1) R_{water}-mod and R_{surf}-mod
		(2) Update to z/L and $z = 10\,m$
		(3) DMSO chemistry bug fix

2.4 Ground based observations

We compare the modelled surface SO_2 and SO_4^{2-} concentrations to observations from the Clean Air Status and Trends Network (CASTNet, http://epa.gov/castnet/javaweb/index.html, Finkelstein et al., 2000) and the European Monitoring and Evaluation Program (EMEP, http://ebas.nilu.no/; Torseth et al., 2012). CASTNet provides surface observations of mean seasonal SO_2 and SO_4^{2-} concentrations which are available from 1987 to the present at 97 sites situated in the United States of America (USA). In this study we used observations from the CASTNet sites designated as "western reference" or "eastern reference". The reference sites have been reporting measurements since at least 1990 and are used for determining long term trends, (e.g., Clarke et al., 1997; Holland et al., 1998; MACTEC-Engineering and Consulting, 2005; Baumgardner et al., 2002). There are 16 western reference sites and 33 eastern reference sites which are located in the continental USA to the west and east of $100°W$ respectively (MACTEC-Engineering and Consulting, 2005). The eastern region is significantly more polluted than the western region due to the larger number of SO_2 sources there. We therefore keep the western and eastern data sets separate to assess how UKESM1 performs in the two regions. Hereafter, we refer to the eastern and western USA regions as USA–E and USA–W, respectively. For this evaluation we used the mean seasonal surface concentrations for SO_2 and SO_4^{2-} which are ~~determined from hourly measurement data~~measured with filter pack samplers at weekly sampling intervals. Details of the quality control procedures and of how the ~~the~~ mean seasonal concentrations are calculated are given in (Baumgardner et al., 2002).

We also evaluate ~~the~~ simulated SO_2 dry deposition flux from UKESM1 against observations from CASTNet, using the same eastern and western reference sites that were used to evaluate surface SO_2 and SO_4^{2-} concentrations. The CASTNet deposition fluxes are derived using modelled deposition velocities rather than directly measured fluxes, which are difficult to obtain due to the requirement for extensive instrumentation and technical resource. Direct measurements of SO_2 dry deposition flux are therefore temporally and spatially limited, and not suitable for evaluating long term trends. To derive the SO_2 dry deposition fluxes, measurements of SO_2 concentration are combined with routine meteorological measurements, information on the land use type and LAI at the measurement site. This data is then combined with modelled deposition velocities from the Multi Layer Model (MLM, Meyers et al., 1998; Saylor et al., 2014). The methodology used to derive the SO_2 dry deposition fluxes for CASTNet is described in ~~Clarke et al. (1997); Baumgardner et al. (2002)~~Clarke et al. (1997) and Baumgardner et al. (2002). While the modelled SO_2 dry deposition fluxes can be under-predicted by approximately 30% (Clarke et al., 1997), it is considered to be the best available approach to regional scale assessment of dry deposition (Finkelstein et al., 2000; Baumgardner et al., 2002; E. Sickles and Shadwick, 2007; Sickles and Shadwick, 2007). This approach has been used to determine SO_2 dry deposition fluxes for CASTNet since 1987 (e.g., Clarke et al., 1997; Baumgardner et al., 2002) and to assess global and regional scale models (Vet et al., 2014; Tan et al., 2018; Tang et al., 2018).

Surface SO_2 and SO_4^{2-} concentrations have been monitored at EMEP sites for the period 1972 – present (Torseth et al., 2012). In this study we have used observations of surface concentration of SO_2 and SO_4^{2-} from ~~144 and 99 sites respectively,~~

~~although not all sites have measurements over the full period~~ 48 and 42 sites respectively. We have selected sites where there are at least 10 years of continuous measurements and with a few exceptions have used sites where SO_2 and SO_4^{2-} were co-located. We use monthly mean observations for both species. No SO_2 dry deposition data were available from EMEP. The locations of the CASTNet and EMEP sites used in this study are shown in Figure 1.
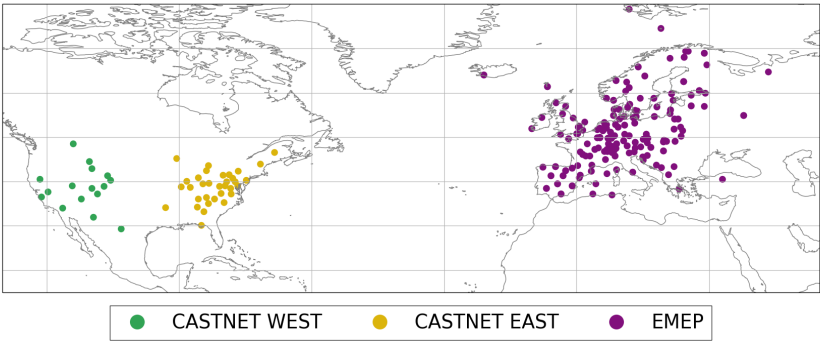
325

Figure 1. Map of the locations of the CASTNet and EMEP measurement sites used in this study.

2.5   Data processing

For this evaluation we calculated seasonal averages for the modelled surface SO_2 and SO_4^{2-} concentrations and for the EMEP observational data. The seasonal periods were defined as December-January-February (DJF), March-April-May (MAM), June-July-August (JJA) and September-October-November (SON). The CASTNet data for all variables was available as seasonal

330   averages for these periods. Model grid cell output was co-located with the CASTNet and EMEP measurement sites. In some cases, this resulted in model data from a particular grid cell being compared with more than one measurement site. For the time series analysis, regional means and standard deviations were calculated across the sites in the USA-E, USA-W and ~~EMEP~~ Europe regions. Although there is spatial variation in the surface SO_2 and SO_4^{2-} concentrations across Europe, for example concentrations are relatively low in Scandinavia, but are much higher in South East Europe, it is less easy to classify "clean"

335   and "polluted" regions at the global model scale. Therefore we classify Europe as a single region. For the spatial analysis and calculation of time series statistics, we calculate mean values over the whole time series, i.e. 1987-2014 and for two time slices at the start (1990-1995) and end of the time series (2009-2014). For the time slices we only used sites that had at least three out of five years data available. We investigate the two time slices to assess the model's performance during the different pollution levels at the start and end of the ~~the~~ time series. We determine the rate of change (trend) in the surface concentrations

340   by calculating the linear regression for 1987-2014, 1990-1995 and 2009-2014.

2.6 Satellite observations

Total column SO_2 (TCSO$_2$) measurements came from the Ozone Monitoring Instrument (OMI) ~~, which~~ and were obtained from the Goddard Earth Sciences Data and Information Services Centre (https://aura.gesdisc.eosdis.nasa.gov/data/Aura_OMI_Level2/OMSO2.003) (Li et al., 2020). OMI is situated on-board NASA's polar-orbiting Aura satellite launched in 2004 with a local overpass time of approximately 13:45. OMI has a nadir footprint of $13\,km \times 24\,km$ and a spectral viewing range of 270 to 500 nm (Levelt et al., 2018). The TCSO$_2$ product is quality controlled for cloud radiation fraction > 0.0 and < 0.5, solar zenith angle $< 65°$, the South Atlantic Anomaly flag $= 0$, ice cover flag $= 0$, the air mass factor (AMF) > 0.3 and TCSO$_2$ > -1.0 Dobson unit (DU). Background TCSO$_2$ average values tend to be positive near-zero quantities (i.e. just above 0.0), where some soundings are slightly negative. If only positive TCSO$_2$ were incorporated in the background averages, this would positively skew the true value.

For a robust comparison between model simulations and satellite data ~~, to reduce sampling (representation) errors,~~ both data sets typically require spatio-temporal co-location to reduce sampling (representation) errors. To achieve this, high temporal resolution (e.g. 3 hourly or 6 hourly) model output of 3D tracer and pressure fields are required over the analysis period to capture e.g. diurnal variability (Pope et al., 2016; Monks et al., 2017). However, this is difficult when using standard climate model simulations, including those used in this study, which typically output monthly means due to their long term climate focus. In this comparison we performed tests to show that using the monthly mean model output was suitable given the relatively uniform diurnal cycle of SO_2 emissions. For these tests we made initial comparisons of model output and satellite data using 6 hourly and monthly mean output from the same UKESM1 simulation. We found that the temporal sampling of the model was not overly critical for SO_2, i.e. modelled SO_2 has a sufficiently long lifetime to dampen the influence of diurnal sampling of the model. Further details on the TCSO$_2$ product, how it was processed to obtain TCSO$_2$ values and the assessment of the temporal resolution is given in Pope and Chipperfield (2021).

3 Evaluation of trends and biases in modelled SO_2 and SO_4^{2-} concentrations

3.1 Time series analysis of surface concentrations of SO_2 and SO_4^{2-} ~~for 1987–2014~~

UKESM1 simulations of surface of SO_2 and SO_4^{2-} concentrations are compared with observations from the CASTNet and EMEP networks for the period 1987–2014 in Figure 2. The statistics summarizing the model bias and trends over this period as well as for the 1990–1995 and 2009–2014 time slices are shown in Tables 3 and 4. We find that UKESM1 captures the historical reduction in surface SO_2 and SO_4^{2-} concentrations~~, but was less able to simulate the finer detail in the temporal trends~~. This is in agreement with Aas et al. (2019) who reported that an ensemble of global aerosol models were generally able to capture the recent historical declines in these two species over the USA and Europe. UKESM1 over-predicts surface SO_2

concentrations in all three regions, but the direction of the model's bias in surface SO_4^{2-} concentrations is spatially variable.
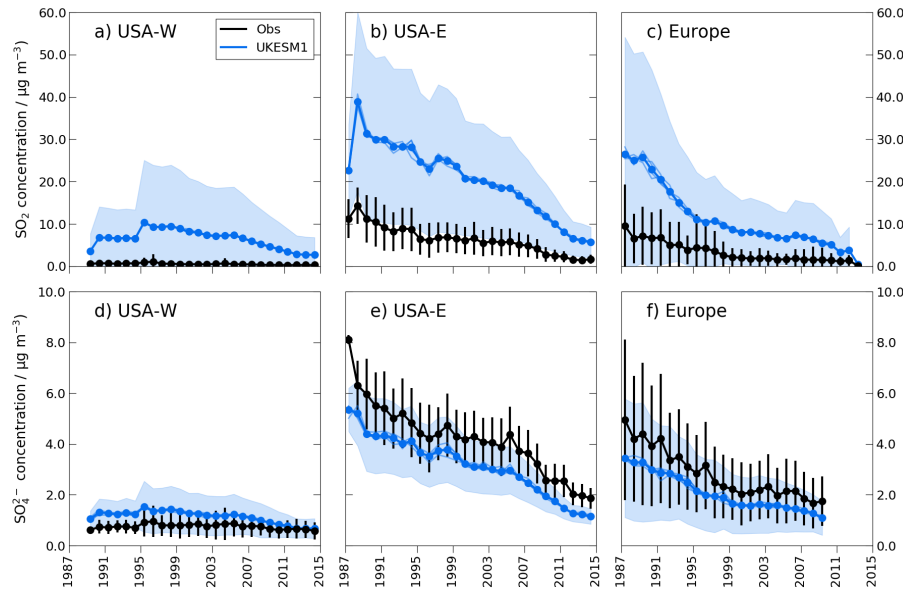

Figure 2. Time series of observed and modelled mean annual surface SO_2 (top row) and SO_4^{2-} (bottom row) concentrations for USA–W (a, ~~cd;~~ N sites = 16), USA–E (b, ~~de;~~ N sites = 33) and Europe (c, ~~ef;~~ N sites = 48 for SO_2 and 42 for SO_4^{2-}). Each point in the time series represents the mean across the measurement sites in the region. Note that the vertical scale for SO_2 (a-c) is a factor of 6 larger than that for SO_4^{2-} (d-f).

375   Figures 2a-c show that in both Europe and USA–E the ~~modelled~~ model over-predicts surface SO_2 concentrations~~are over-predicted~~, particularly at the start of the time series, ~~and~~ which then decrease too rapidly. Over Europe, the observed surface SO_2 concentrations decrease at a rate of $0.72\,\mu g\,m^{-3}\,y^{-1}$ in the period 1990–1995 which slows to $0.38\,\mu g\,m^{-3}\,y^{-1}$ by 2009–2014. However, the modelled surface SO_2 concentrations decrease ~~much too rapidly at the start of the time series, reducing~~ by $2.52\,\mu g\,m^{-3}\,y^{-1}$ for 1990–~~1995. This slows to~~ 1995, slowing to only $-1.31\,\mu g\,m^{-3}\,y^{-1}$ by 2009–~~2014, but is still too rapid~~

380   ~~compared to the observations.~~ 2014. Over USA–E the observed surface SO_2 concentrations decrease at similar rates ~~of between 0.36 $\mu g\,m^{-3}\,y^{-1}$ and 0.25 $\mu g\,m^{-3}\,y^{-1}$~~ at the start and end of the time series. UKESM1 ~~does capture this~~ is better able to capture the trend at the start of the time series, but simulates a too rapid reduction in surface SO_2 concentrations after 2005 (see Figure 2b). Over USA–E UKESM1 simulates the sharp drop in surface SO_2 concentrations that occurred in 1995 following the implementation of Phase 1 of the USA's Clean Air Act Amendments (McHale et al., 2021). However, ~~following this event the model~~

385   the model then simulates relatively high surface SO_2 concentrations for the period ~~1997~~1996–1999, rather than the sustained lower surface SO_2 concentrations that are observed after 1995. ~~In~~ Over USA–W the observed surface SO_2 concentrations remain steady from 1987 to 2014 due to there being fewer sources in this region. Figure 2a shows that UKESM1 simulates

14

the steady surface SO_2 concentrations at the start of the time series, albeit with a positive bias. However, after 1995 UKESM1 simulates decreasing surface SO_2 concentrations in USA–W, which brings the modelled values in to better agreement with the

390   observations, but introduces an artificial trend into the modelled time series.

UKESM1 over-predicts the annual mean surface SO_2 concentrations in the polluted regions of Europe and USA–E by a factor of 3.2 to 3.4 over the period 1987–2014, although the absolute bias is higher USA–E (see Table 3). While the absolute magnitude of the bias in mean annual surface SO_2 concentration is less in USA–W compared with the polluted regions, pro-

395   portionally it is much larger, with the model simulating surface SO_2 concentrations more than 10 times the observed values. The absolute magnitude of the bias in mean annual surface SO_2 concentration decreased from 1990–1995 to 2009–2014 in all three regions (see Table 3) reflecting the model's more rapid decrease in surface SO_2 concentrations relative the observations. However, the NMB values were slightly higher in 2009–2014 compared with 1990–1995.

$\approx$ Figure 2c-f show that UKESM1 reproduces both the magnitude and the trends in surface SO_4^{2-} concentrations in the polluted regions of U to better than the surface SO_2 concentrations. The model simulated surface SO_4^{2-} concentrations decreasing at a rate of ~~0.14~~ 0.13 $\mu g \, m^{-3} \, y^{-1}$ (USA–E) and ~~0.12~~ 0.09 $\mu g \, m^{-3} \, y^{-1}$ (Europe) compared with the observed trend of ~~0.16~~
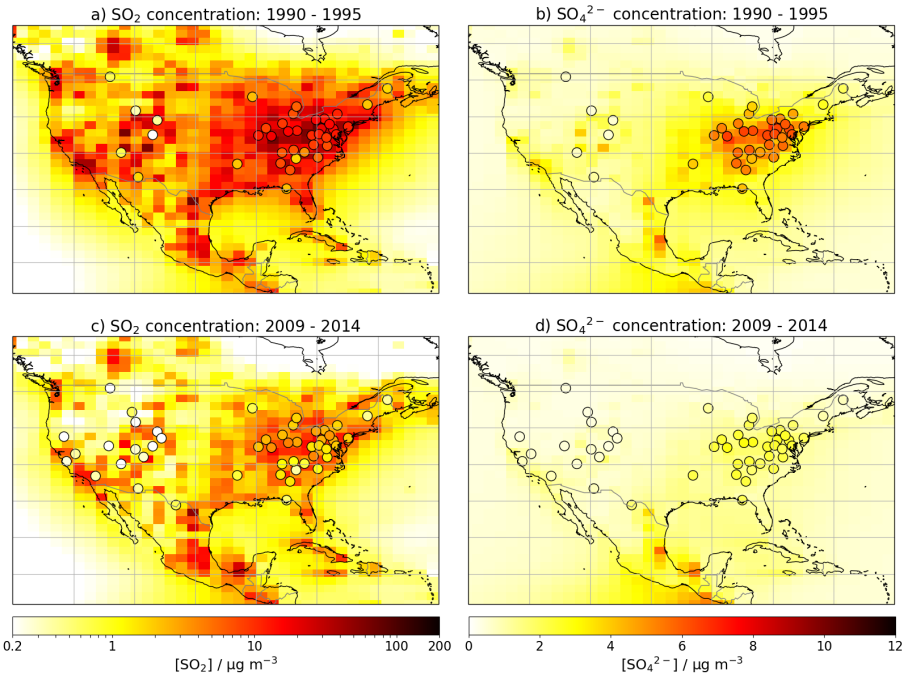

Figure 3. Mean annual surface SO_2 concentration (a, c) and surface SO_4^{2-} concentration (b, d) for 1990–1995 (top row) and 2009–2014 (bottom row) for modelled output. Observations from 49 CASTNet measurement sites are plotted as black-edged circles on the same colour scale.

Table 3. Statistics for mean annual surface SO_2 concentrations at USA–W, USA–E and Europe. The mean and trend values are in $\mu g\,m^{-3}$ and $\mu g\,m^{-3}\,y^{-1}$ respectively.

		1987–2014	1990–1995	2009–2014
USA–W	Mean (obs)	~~0.53~~ 0.48	~~0.71~~ 0.67	0.29
	Mean (model)	~~6.45~~ 6.48	~~7.29~~ 6.67	~~3.40~~ 3.19
	Bias	~~5.92~~ 6.00	~~6.58~~ 6.00	~~3.11~~ 2.90
	NMB	~~11.57~~ 12.54	~~9.25~~ 9.00	~~10.63~~ 10.04
	R	~~0.81~~ 0.20	~~0.88~~ 0.89	~~0.22~~ 0.93
	Trend (obs)	~~-8.39~~ -7.13$\times10^{-3}$	~~-1.45~~ -1.46$\times10^{-2}$	~~-4.89~~ -2.05$\times10^{-3}$
	Trend (model)	~~-4.12~~ -4.58$\times10^{-2}$	-5.74$\times10^{-2}$	~~-0.34~~ -0.36
	N sites	16	6	16
USA–E	Mean (obs)	~~6.31~~ 6.34	~~8.64~~ 9.09	~~2.02~~ 1.87
	Mean (model)	~~20.36~~ 20.05	~~28.22~~ 28.89	~~8.04~~ 7.28
	Bias	~~14.06~~ 14.20	~~19.58~~ 19.90	~~6.02~~ 5.41
	NMB	~~2.23~~ 2.41	~~2.27~~ 2.20	~~2.99~~ 2.92
	R	~~0.94~~ 0.97	~~0.93~~ 0.89	~~0.96~~ 0.94
	Trend (obs)	-0.37	-0.36	~~-0.24~~ -0.25
	Trend (model)	~~-0.98~~ -1.00	~~-0.52~~ -0.53	~~-1.05~~ -1.04
	N sites	33	33	33
Europe	Mean (obs)	~~3.29~~ 2.94	~~5.28~~ 4.96	~~1.09~~ 1.27
	Mean (model)	~~11.12~~ 10.20	~~16.69~~ 15.80	~~3.62~~ 4.38
	Bias	~~7.83~~ 7.26	~~11.41~~ 10.90	~~2.53~~ 3.12
	NMB	~~2.38~~ 2.61	~~2.16~~ 2.27	~~2.32~~ 2.47
	R	~~0.97~~ 0.93	~~0.92~~ 0.99	0.97
	Trend (obs)	~~-0.27~~ -0.20	~~-0.72~~ -0.42	~~-0.38~~ -0.02
	Trend (model)	~~-0.84~~ -0.66	~~-2.52~~ -1.35	~~-1.31~~ -0.27
	N sites	48	43	47

Figures 3 and 4 show the spatial distribution of modelled and observed mean annual surface SO_2 and SO_4^{2-} concentrations for the periods 1990–1995 and 2009–2014 for the USA and Europe. We find that UKESM1 captures the spatial distribution of surface SO_2 and SO_4^{2-} concentrations over each region, simulating higher concentrations in USA–E, central Europe and eastern Europe where there are numerous large sources, and lower concentrations in USA–W and northern Europe which have much fewer sources ~~and are relatively clean~~ (see Figure B1). These figures also show the localised versus dispersed nature of the surface SO_2 and SO_4^{2-} concentrations, with high SO_2 concentrations located within $2-3$ grid boxes ($200-400\,km$) of the

405

Table 4. Statistics for mean annual surface SO_4^{2-} concentrations at USA–W, USA–E and Europe. The mean and trend values are in $\mu g\,m^{-3}$ and $\mu g\,m^{-3}\,y^{-1}$ respectively.

		1987–2014	1990–1995	2009–2014
USA–W	Mean (obs)	0.74	0.73	0.62
	Mean (model)	1.15	1.27	0.73
	Bias	0.44	0.54	0.11
	NMB	0.72	0.73	0.18
	R	0.14	0.7	0.90
	Trend (obs)	-1.01×10^{-2}	-3.41×10^{-3}	-9.45×10^{-3}
	Trend (model)	-5.83×10^{-3}	-1.41×10^{-2}	-3.97×10^{-2}
	N sites	16	6	16
USA–E	Mean (obs)	3.82	5.17	2.18
	Mean (model)	3.14	4.21	1.38
	Bias	-0.67	-0.96	-0.80
	NMB	-0.19	-0.19	-0.37
	R	0.98	0.87	0.94
	Trend (obs)	-0.10	-0.13	-0.2
	Trend (model)	-0.13	-0.07	-0.14
	N sites	33	33	33
Europe	Mean (obs)	2.76	3.81	1.75
	Mean (model)	1.91	2.86	1.06
	Bias	-0.85	-0.94	-0.69
	NMB	-0.31	-0.24	-0.39
	R	0.97	0.91	0.74
	Trend (obs)	-0.12	-0.29	-0.09
	Trend (model)	-0.09	-0.09	-0.03
	N sites	42	41	34

emission sources (see Figure B1), while SO_4^{2-} is distributed more widely. ~~UKESM1 is also able to simulate the range of concentrations obs~~
3 shows that modelled and observed surface SO_2 and SO_4^{2-} concentrations across the USA are lower in 2009–2014 compared with 1990–1995 demonstrating the ~~impact of emissions reductions policy across the USA, which the model also simulates well~~ widespread
However, the ~~divide~~ disparity between higher concentrations in USA–E ~~compared with~~ and lower concentrations in USA–W is still apparent for both species in the later period.

south east (SE) of England (see Figure 4). Lower concentrations of both species were observed in ~~Scandinavia, the Iberian~~
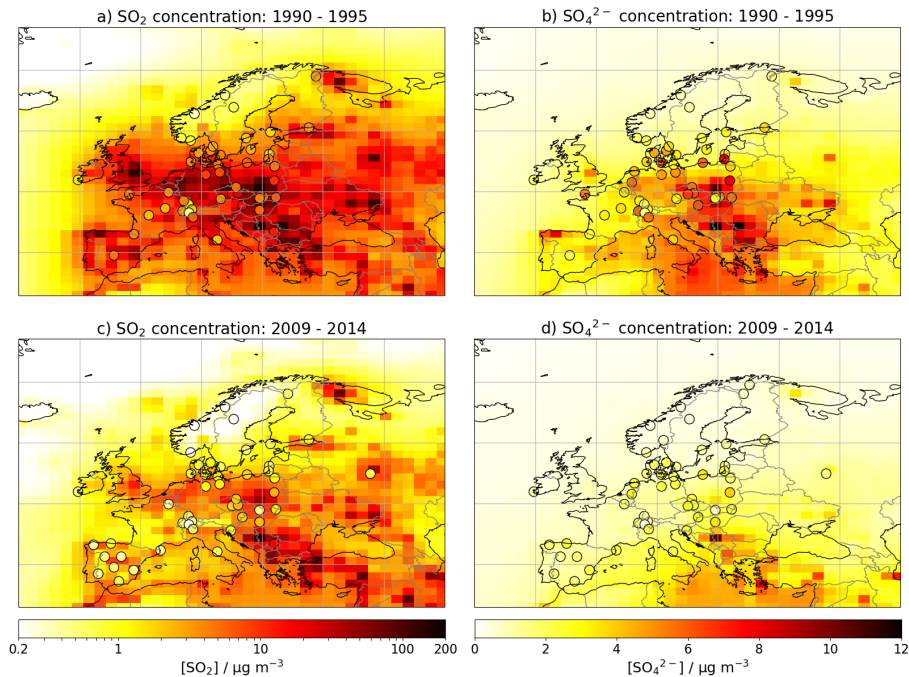
Figure 4. Mean annual surface SO_2 concentration (a, c) ~~for 1990–1995 (a)~~ and ~~2009–2014 (b);~~ surface SO_4^{2-} concentration (b, d) for 1990–1995 (~~b, no data available for~~ top row) and 2009–2014 (bottom row) for modelled output. Observations from EMEP measurement sites (N sites $= 48$ for SO_2 and 42 for SO_4^{2-}) are plotted as black-edged circle on the same colour scale.

415   ~~peninsular, south west France and at Mace Head on~~ northern and western regions, e.g. Scandinavia and the west coast of Ireland. Figure 4c shows that mean annual surface SO_2 concentrations were ~~uniformly~~ generally lower in 2009–2014 compared with 1990–1995, especially in Central and Eastern Europe, due to the impact of air quality legislation~~over the last 30 years~~. However, for 2009–2014 modelled and observed levels of SO_2 remain high in the south eastern region (see Figure 4c). UKESM1 reproduces the spatial distribution of mean annual SO_2 ~~concentration~~concentrations across Europe, but has large positive biases over

420   most of the region. The largest model biases were in ~~Eastern and SE Europe from~~ eastern and south eastern Europe during the period 1990–1995 where UKESM1 simulates mean annual surface SO_2 concentrations of up to $100\,\mu g\,m^{-3}$ compared with observed values of $10\text{-}30\,\mu g\,m^{-3}$.

     Figure 4b shows that UKESM1 captures the spatial distribution between low mean annual surface SO_4^{2-} concentrations in ~~the~~ northern and western regions of Europe and ~~the~~ high mean annual surface SO_4^{2-} concentrations in central Europe. However,

425   the model under-predicts ~~the spatial extent of the~~ mean annual surface SO_4^{2-} concentrations ~~across Europe. The largest biases of 5 - 7 µg m⁻³ occur in an area including northern Germany, Denmark , southern Sweden, eastern Poland, Switzerland, Belgium and the Netherlands. In comparison, UKESM1 under-predicts mean annual surface SO₄²⁻ concentrations by approximately 2 - 3 µg m⁻³ outside of this area. In Europe SO₂ concentrations are uniformly lower in 2009–2014 compared with 1990–1995, especially in Central and Eastern Europe (see Figures 4a and c). However, the model continues to predict very high levels of~~

430 ~~SO₂ in the SE region for 2009–2014 (see Figure 4c)~~<ins>at many locations across Europe with the largest biases occurring across Denmark and the regions surrounding the Baltic Sea.</ins>

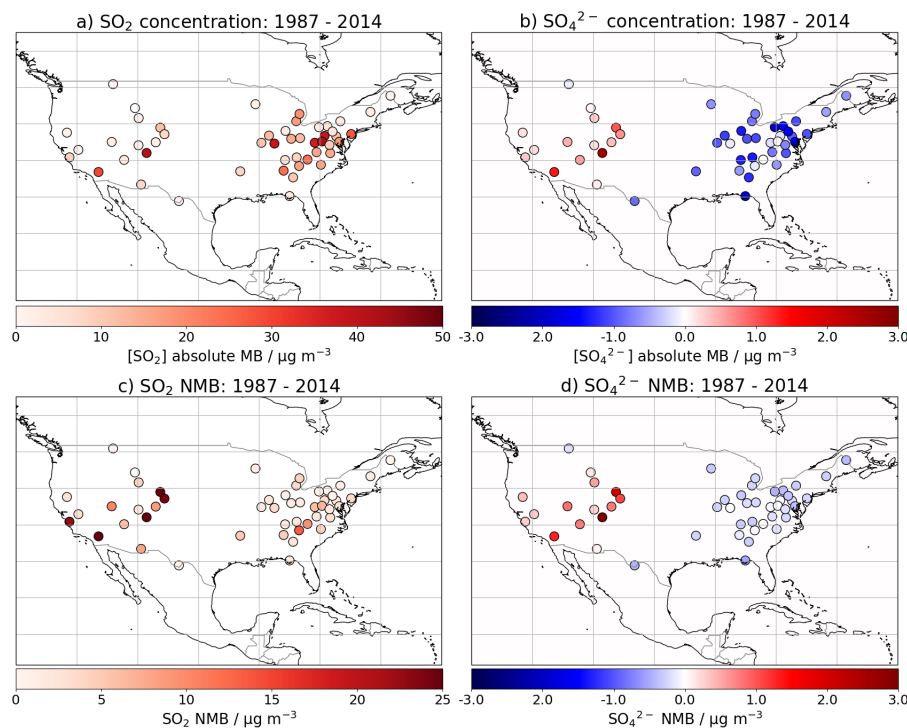## 3.3 Spatial distribution of model bias in surface SO_2 and SO_4^{2-} concentrations

Figure 5. Geographic distribution of mean bias (UKESM1 - obs) in mean annual surface SO_2 and SO_4^{2-} concentration at <ins>49</ins> CASTNet ~~site locations~~<ins>measurement sites</ins>. The mean annual surface concentrations are calculated over the period 1987 to 2014. Absolute mean bias (MB) is shown in (a) and (b) and normalised mean bias (NMB) is shown in (c) and (d). Note that different scales are used for the SO_2 model bias (a) and normalised mean bias (c).

Figures 5 and 6 show that the direction of the model biases<ins>, whether poisitive or negative,</ins> is generally consistent across ~~the regions~~<ins>a region</ins>. UKESM1 over-predicts mean annual surface SO_2 concentration for all sites in both the USA–E and USA–W regions, and with the exception of some Scandinavian sites, across Europe. Figures 5 and 6 also show that mean annual surface SO_4^{2-} concentrations are generally under-predicted across the USA–E and European sites, while being over-predicted at the USA–W sites.
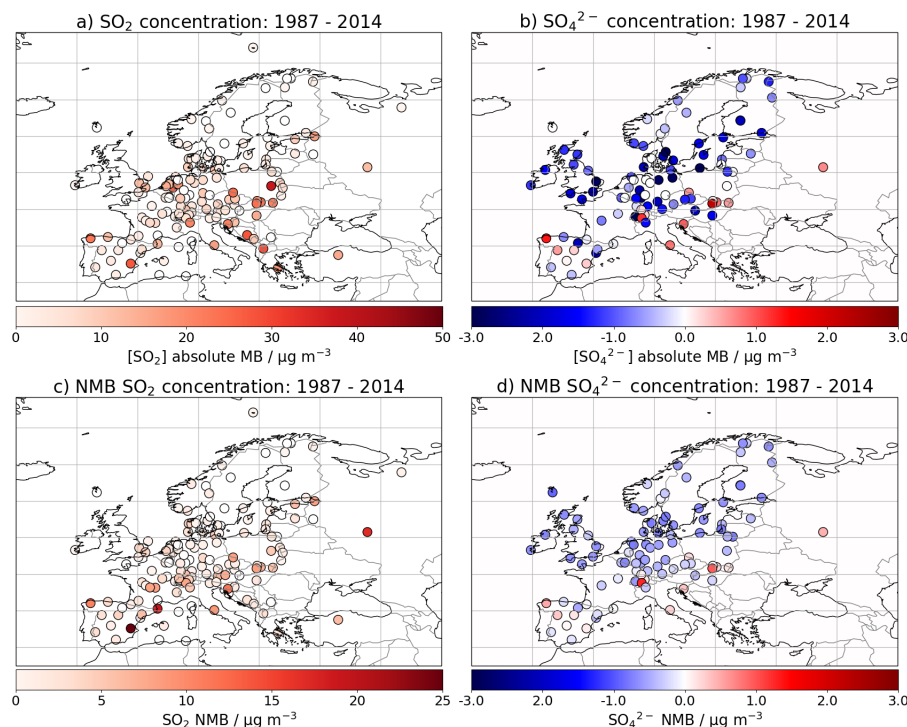
Figure 6. Geographic distribution of mean bias (UKESM1 - obs) in mean annual surface SO_2 and SO_4^{2-} concentration at EMEP ~~site locations~~ measurement sites (N sites $= 48$ for SO_2 and 42 for SO_4^{2-}). The mean annual surface concentrations are calculated over the period 1987 to 2014. Absolute mean bias is shown in (a) and (b) and normalised mean bias (NMB) is shown in (c) and (d). Note that different scales are used for the SO_2 model bias (a) and normalised mean bias (c).

440 The model's over-prediction of mean annual surface SO_2 concentration is largest close to the sources. For example, UKESM1 over-predicts surface SO_2 concentrations by up to $50\,\mu g\,m^{-3}$ in the central USA–E area, but only by around $10\,\mu g\,m^{-3}$ at the surrounding sites. ~~In~~ Whilst in Europe the largest biases of around $10\text{-}20\,\mu g\,m^{-3}$ tend to be ~~distributed across the region due to the more distributed nature of the point sources and on average the model bias is lower than in USA–E~~ in central and eastern areas. The model's tendency to over-predict SO_2 concentrations to a greater extent close to the sources is also shown in the

445 plots of NMB (see Figures 5c and 6c) and is likely why there is a larger range in the modelled mean annual surface SO_2 concentrations averaged across the USA–E and European measurement sites compared with the observational values (see Figures 2b and c). Figures 5b and 6b show that UKESM1 generally under-predicts surface SO_4^{2-} concentration across the USA–E and European sites, with model biases of -1 to $-3\,\mu g\,m^{-3}$. We find that in USA–E the ~~larger negative biases are not directly~~ largest negative biases in surface SO_4^{2-} concentrations are not necessarily co-located with the largest positive biases in SO_2, instead

450 occurring at sites ~~surrounding~~ several hundred kilometres from the large point sources. Similarly, in Europe the largest biases in surface SO_4^{2-} concentrations occur further north than the large biases in surface SO_2 concentration, and in certain sites located

20

near large sources, UKESM1 over-predicts surface SO_4^{2-} concentrations. The plots of NMB show that there is less spatial variation in the model bias for surface SO_4^{2-} concentrations reflecting UKESM1's ability to capture the more distributed nature of atmospheric SO_4^{2-}. In USA–W UKESM1 over-predicts both SO_2 and SO_4^{2-} concentrations at almost all of the sites (see Figure 5). For SO_2 this is a consequence of the sparsely distributed measurement sites being located in rural regions remote from any of the sources in USA–W (Clarke et al., 1997; MACTEC-Engineering and Consulting, 2005; Baumgardner et al., 2002) (see also Figure B1). This results in some very large NMB values in USA–W (see Figure 5a).

3.4 Seasonal Cycles
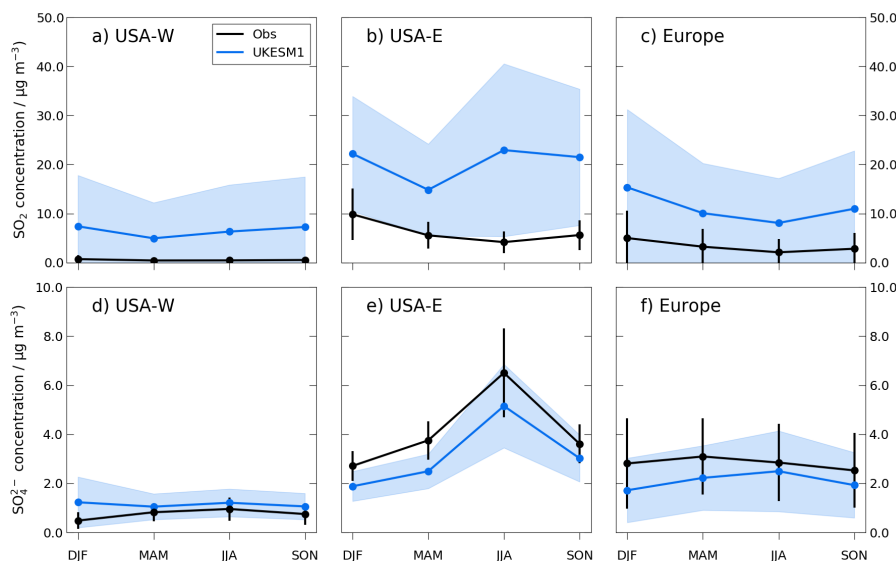
Figure 7. Modelled and observed seasonal mean surface SO_2 concentration (top row) and surface SO_4^{2-} concentration (bottom row) for the period 1987–2014. USA–W, (a, d; N sites = 16); USA–E, (b, e; N sites = 33) and EMEP (c, e; N sites (SO_2) = 48 and N sites (SO_4^{2-}) = 42). The blue shaded region and the black error bars represent the standard deviation across the sites in the observational network.

Figure 7 shows modelled and observed surface SO_2 and SO_4^{2-} concentrations averaged seasonally for the period 1987–2014. The comparison between the model and observations is summarised for DJF and JJA in Table 5. The higher winter time SO_2 concentrations are driven by greater emissions from coal fired power plants and domestic heating, and less oxidation. Conversely there are fewer emissions and higher oxidant concentrations in summer time. These cycles drive correspondingly low SO_4^{2-} concentrations in winter and high SO_4^{2-} concentrations in summer. Overall, we find that the model bias in surface SO_2 and SO_4^{2-} concentrations depends on the season as well as the region and pollution levels.

Table 5. Statistics for seasonal mean surface SO_2 and SO_4^{2-} concentrations ($\mu g\,m^{-3}$) at USA–W, USA–E and Europe. The mean seasonal values are averaged over the period 1987–2014.

	USA–W		USA–E		Europe	
	DJF	JJA	DJF	JJA	DJF	JJA
SO_2 concentration						
Mean (obs)	0.71	0.45	9.83	4.17	5.00	2.10
Mean (model)	7.39	6.32	22.18	22.93	15.34	8.08
Bias	6.69	5.87	12.34	18.76	10.34	5.99
NMB	12.16	12.85	1.37	5.01	2.64	3.09
N sites	16	16	33	33	48	48
SO_4^{2-} concentration						
Mean (obs)	0.48	0.95	2.71	6.51	2.81	2.85
Mean (model)	1.23	1.21	1.88	5.15	1.72	2.50
Bias	0.75	0.25	-0.83	-1.35	-1.09	-0.35
NMB	1.63	0.26	-0.32	-0.22	-0.38	-0.13
N sites	16	16	33	33	42	42

The results presented in Sections 3.1 and 3.1 show that UKESM1 consistently over-predicts mean annual surface SO_2 concentrations in the USA and Europe, however Figures 7a-c show that in the more polluted regions (USA–E and Europe), the magnitude of the bias is seasonal, although still with a large positive bias. UKESM1 is able to capture the seasonal cycle in surface SO_2 concentrations over Europe, but the absolute model bias is larger in DJF compared with JJA (see Table 5). In USA–E UKESM1 does not capture the seasonal cycle in surface SO_2 concentrations due to the relatively large model bias in JJA, where the modelled SO_2 concentrations are over five times the observed values. In ~~contrast the model over-predicts surface SO_2 concentrations in DJF by a factor of 2.3. In~~ USA–W the modelled and observed surface SO_2 concentrations are slightly higher in DJF compared with JJA~~. The model bias is also larger in DJF compared with JJA~~, but the ~~SO_2 concentrations are over-predicted to such a large degree~~ model bias is so large in this region that it is difficult to determine if there is any seasonality in this bias.

UKESM1 clearly captures the seasonal cycle in surface SO_4^{2-} concentration over USA–E, simulating the highest values in summer and the lowest values in winter. The model under-predicts surface SO_4^{2-} concentration by a factor of 0.7 to 0.8 reasonably consistently throughout the seasonal cycle. In the cleaner USA–W region, UKESM1 is able to capture the seasonal cycle in surface SO_4^{2-} concentrations, with the exception of DJF where the model over-predicts surface SO_4^{2-} concentrations by a factor of 2.5. In Europe the observed seasonal cycle in surface SO_4^{2-} concentration has only a small amplitude with mean

values of 2.81 μg m^{-3} and 2.85 μg m^{-3} in DJF and JJA respectively.

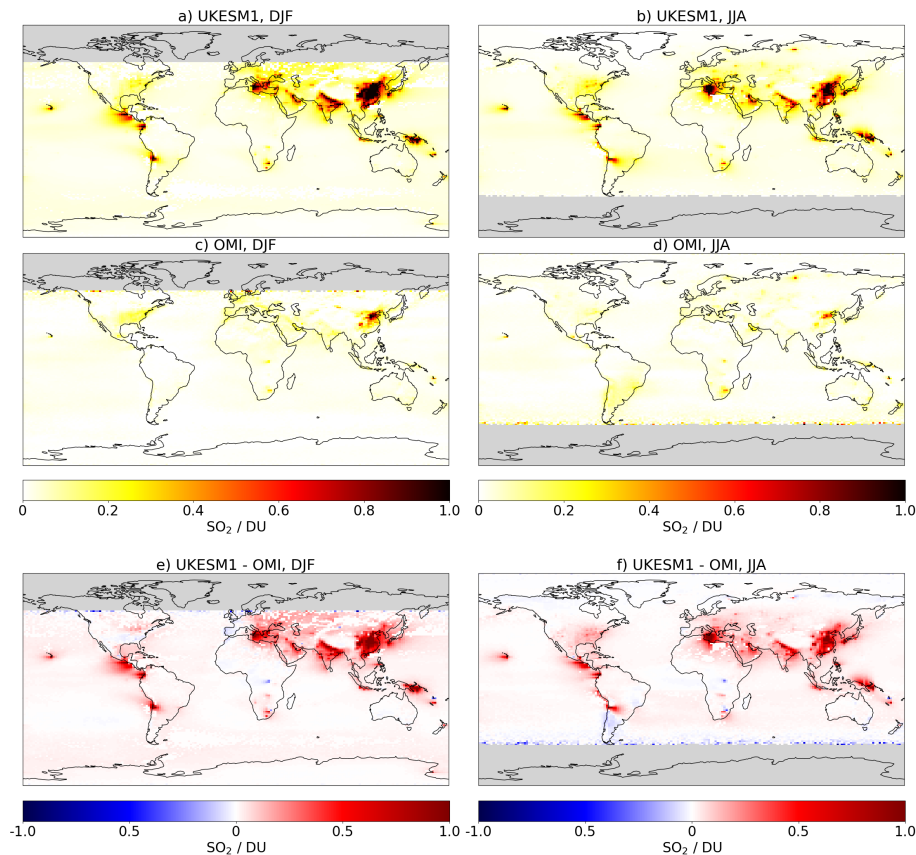## 3.5 Evaluation of total column SO$_2$ in UKESM1 against satellite observations

Figure 8. ~~Median~~ Total Column SO$_2$ ~~(Dobson Units)~~ for ~~2005 to 2014 for~~ UKESM1 (a, b) OMI (c, d) and UKESM1 – OMI (e, f). DJF is shown in the left column and JJA is shown in the right column. Median Total Column SO$_2$ in Dobson Units is calculated for the period 2005–2014.

Figure 8 shows total column SO$_2$ (TCSO$_2$) from UKESM1 and OMI, and the difference between them for DJF and JJA. Note that the quality control for solar zenith angle results in no data availability above 65°N degrees or below 65°S in the winter months, and due to OMI's weaker sensitivity to retrieving SO$_2$ in remote regions we focus on comparing TCSO$_2$ over source and outflow regions (Li et al., 2020). Figures 8 a-d show that UKESM1 and OMI broadly agree on the location of the main northern hemisphere (NH) source regions including China, India, Europe and the USA. The model and satellite data both show seasonal cycles in TCSO$_2$ over the large source regions with higher values being modelled and observed during
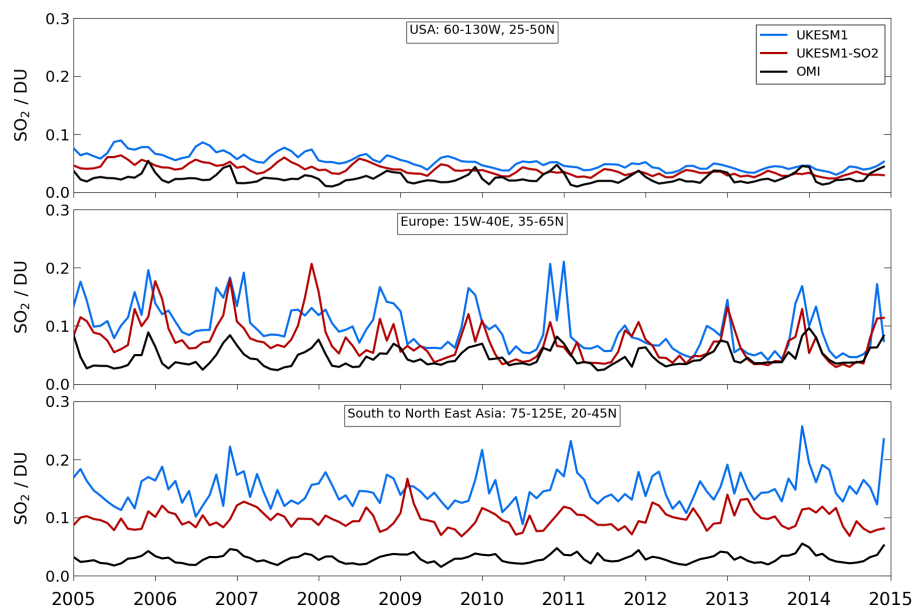
23

Figure 9. Median Total Column SO$_2$ ~~(Dobson Units)~~ calculated for 2005~~to~~–2014 for USA, (a); Europe, (b); and South to North East Asia, (c). Total Column SO$_2$ is in Dobson Units.

Table 6. Statistics ~~between~~ comparing model ~~runs~~ and OMI ~~TC~~Total Column SO$_2$ ~~monthly zonally averaged (median) time series (2005-2014) for~~ over three ~~latitude bands~~ regions; USA (60 – 130°W, 25 – 50°N)~~;~~, Europe (15°W – 40°E, 35 – 65°N) ~~;~~ and South to North East Asia (75 – 125°W, 20 – 45°N) for the period 2005-2014. The metrics ~~include the~~ are mean bias (MB, DU), root mean square error (RMSE, DU), percentage mean bias (MB%) and correlation (R).

	USA		Europe		South to North East Asia	
Statistic	UKESM1	UKESM1-SO2	UKESM1	UKESM1-SO2	UKESM1	UKESM1-SO2
MB	0.029	0.014	0.050	0.027	0.120	0.068
RMSE	0.032	0.018	0.061	0.040	0.122	0.070
MB%	117	56	110	59	402	228
R	0.26	0.19	0.54	0.53	0.64	0.48

Note that the median value is reported for each metric.

the winter months. However, Figures 8 e and f show that the UKESM1 TCSO$_2$ values were generally larger than the OMI TCSO$_2$ values in these source regions by 0.6 – 1.0 Dobson Units (DU). Over the background regions UKESM1 over-predicts TCSO$_2$ values by 0.2 – 0.5 DU. UKESM1 also has larger volcanic sources and associated outflow, which can be seen over central America, Sicily, Hawaii and Papua New Guinea, for example. This is likely due to the climatology that UKESM1 uses for continuously degassing volcanoes. In agreement with the ground based observations, the satellite data shows an ~~East-West~~

east-west divide in the USA, with greater $TCSO_2$ over USA–E compared with USA–W.

Figure 9 shows modelled and observed $TCSO_2$ over the period from 2005 to 2014 for three source regions, the USA (60–30°W, 25–50°N), Europe (15°E–40°E, 35–65°N) and South to North East (SNE) Asia (75–125°E, 20–45°W). Overall, we find that the observed $TCSO_2$ is reasonably stable over this period in all three regions and that there are clear seasonal cycles showing peak $TCSO_2$ during the NH winter in the USA and Europe, and slightly earlier in SNE Asia. However, Figures 9a and b show that modelled $TCSO_2$ decreases over the USA and Europe from 2005–2010 with UKESM1 over-predicting $TCSO_2$ by up to 0.1 DU at the start of the time series. After 2011, UKESM1 is in much better agreement with the observed $TCSO_2$ over both regions. Figure 9c shows that UKESM1 consistently over-predicts $TCSO_2$ over SNE Asia by 1.5–2.0 DU during the period from 2005 to 2014. UKESM1 does simulate a seasonal cycle in $TCSO_2$ in all three regions. In Europe, UKESM1 is able to predict the peak winter time $TCSO_2$ values, although between 2005–2010 the model has a positive bias of up to 0.1 DU. However, in the USA and to a lesser extent in SNE Asia (Figures 9 a and c respectively), UKESM1 mis-times the peak $TCSO_2$ values. In the USA the model simulates the highest values in the summer rather than in winter, and in SNE Asia the modelled peak $TCSO_2$ values appear shifted several months earlier ~~in relation~~ relative to the observations.

The observations of $TCSO_2$ and surface SO_2 concentrations over Europe both show the impact of emission control policies on keeping atmospheric SO_2 levels low ~~and stable (see~~ (Figures 2c and 9b). ~~For~~ However, for the USA, we investigate the surface SO_2 concentrations separately over the USA–E and USA–W regions, whereas the $TCSO_2$ is averaged over ~~the whole continental USA~~ continental USA as a whole. As a result ~~, the trend for decreasing~~ $TCSO_2$ does not appear to decrease over the period 2005–2014 in the same way surface SO_2 concentrations ~~are reduced~~ in USA–E (~~see Figure 2b) is not seen in TCSO_2~~ Figures 2b and 9a). Using a mean $TCSO_2$ for the continental USA as a whole also results in lower values relative to Europe. This is in contrast to the ground-based observations where surface SO_2 concentrations over Europe are intermediate between USA–E and USA–W for the period 2005–2014. The relatively high $TCSO_2$ over Europe is also due to the inclusion of a number of large eastern European sources which are not well represented in the ground based observations. We find that the $TCSO_2$ and surface SO_2 concentration observations both agree on the seasonal cycle, showing higher values in winter compared with the summer.

UKESM1 over-predicts surface SO_2 concentration to a greater extent than $TCSO_2$ for the USA and Europe. The model over-predicts surface SO_2 concentration by a factor of 2.2 - 11.6 for USA–E and USA–W, and 2.4 for Europe compared with values of 1.2 (USA) and 1.1 (Europe) for modelled $TCSO_2$ (see Tables 3 and 6). However, the R values for surface SO_2 concentration (>0.8) are much better than those for $TCSO_2$ (0.26 - 0.53), particularly over the USA. The low R value for the USA reflects the poor seasonal agreement in $TCSO_2$ in this region. The comparison against both observational data sets shows that the modelled atmospheric SO_2 is too high, both at the surface and through the column. In addition, UKESM1 ~~predicts~~ simulates larger trends in $TCSO_2$ and surface SO_2, particularly prior to 2010, ~~that with the exception of USA–E are not~~ than are seen in the observations. Both observational data sets also show that UKESM1's over-prediction of atmospheric SO_2 ~~is~~

in the large source regions is generally greater in the winter months compared to the summer months ~~over the large source regions, with exceptions in USA–E and the Iberian peninsular~~ (see Figures ~~9~~8e and f). ~~In~~ Exceptions occur in USA–E ~~the comparison against the observational data sets shows that~~ where UKESM1 fails to capture the seasonal cycle in atmospheric
SO$_2$, ~~with the model simulating values that are too high~~ over predicting surface SO$_2$ concentration and TCSO$_2$ to a greater extent in JJA compared to DJF. ~~In~~ Notably, in the southern USA–E region and the Iberian ~~peninsular we see that~~ peninsula UKESM1 actually under-predicts TCSO$_2$ by up to 0.1 DU in DJF, which does not occur in the comparison with surface SO$_2$ concentrations, even if the model and observations are compared at individual CASTNet and EMEP sites.

4 Impact of changes to the SO$_2$ dry deposition parameterization in UKESM1

4.1 Global scale impacts
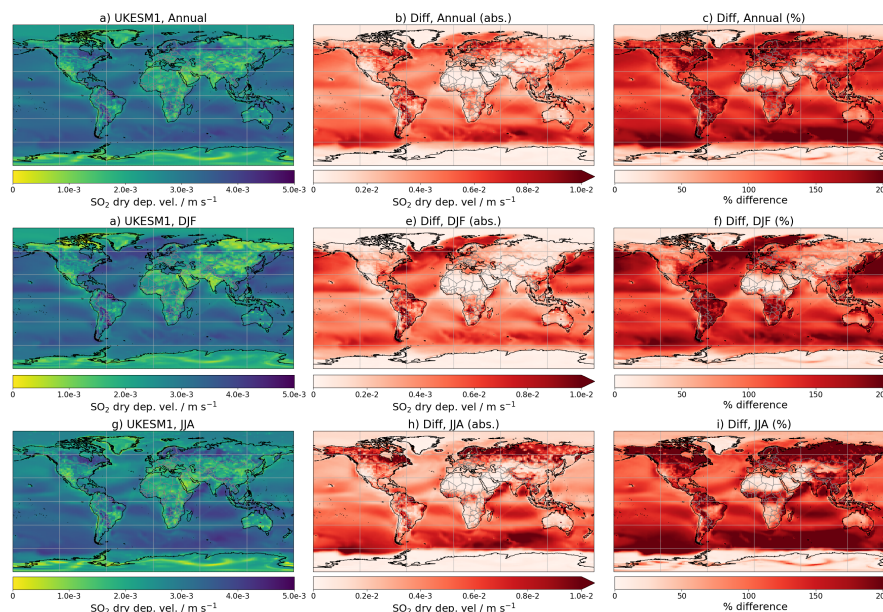
Figure 10. SO$_2$ dry deposition ~~, (a–c); surface SO$_2$ concentration, (d–f) and surface SO$_4^{2-}$ concentration (g–i)~~ velocity for UKESM1, (left column)~~, ;~~ absolute difference in SO$_2$ dry deposition velocity for UKESM1-SO2 - UKESM1, (middle column) and percentage difference in SO$_2$ dry deposition velocity for UKESM1-SO2 - UKESM1, (right column). Annual means are shown in a–c, the DJF mean is hown in d–f and the JJA mean is shown in g–i). Each plot shows mean data for the period 1987–2014. Deposition velocity is calculated from the simulated surface SO$_2$ and dry deposition flux values and represents the 'bulk' deposition velocity for each model grid cell.
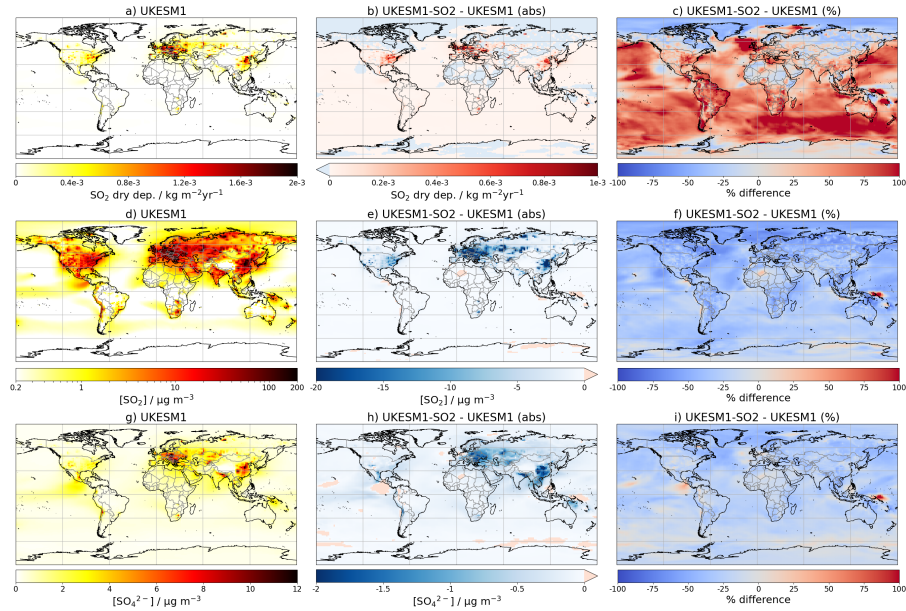
Figure 11. SO_2 dry deposition, (a–c); surface SO_2 concentration, (d–f) and surface SO_4^{2-} concentration (g–i) for UKESM1 (left column), absolute difference for UKESM1-SO2 - UKESM1 (middle column) and percentage difference for UKESM1-SO2 - UKESM1 (right column). In the plots showing absolute difference, areas where SO_2 dry deposition is reduced in UKESM1-SO2 compared with UKESM1 are shown in blue (b) and areas where surface SO_2 and SO_4^{2-} concentration are greater in UKESM1-SO2 compared with UKESM1 are shown in red (e, h). The blue and red shading in (b) and (e, h) is not to scale as the absolute differences are very small. Each plot shows mean data for the period 1987–2014.

Figure ~~11 shows the impact of the modified~~ 10 shows SO_2 dry deposition ~~parameterization on global~~ velocity simulated by UKESM1 and how this is affected by changes to the SO_2 dry deposition ~~, surface~~ parameterization. In UKESM1 the mean annual deposition velocities range from approximately 0.5×10^{-3} to 4.0×10^{-3} (see Figure 10a). Figures 10b, e, and h show that $SO_2 and SO_4^{2-} concentrations for the period 1987 ̆ 2014. Figures 11b and c show dry deposition velocity increases over almost all la$ This represents a factor 2 - 4 increase relative to UKESM1. The largest increase in SO_2 dry deposition velocity to the ocean is over the Southern Ocean in winter where it increases by more than a factor of four (see Figure 10i). Over land surfaces the largest increases occur over South America, north western America and Canada, and north eastern Europe/western Russia (see Figures 10f and i). The increased SO_2 dry deposition velocities in UKESM1-SO2 relative to UKESM1 indicate $that the changes to the SO_2 dry deposition parameterization are behaving as expected$ by increasing. $The reduction in$ R_c for $SO_2 dry deposition. The largest absolute increases of up to 3 \times 10^{-3} to water increases the dry deposition velocity to oceans. Similarly,$ and R_{soil} are reduced for a longer period of time in UKESM1-SO2 relative to UKESM1 and SO_2 dry deposition velocity to the canopy (leaf or soil) increases. In the summer months SO_2 dry deposition velocities are larger over land surfaces compared with in the winter months, while over oceans values are larger in the winter compared with the summer. Although increased

27

rainfall in winter drives wetter surface conditions, the leaf canopy is reduced or absent, and at high latitudes surfaces are likely to have snow cover which has a relatively high R_c (see Table A1) compared with vegetated surfaces. The higher SO_2 dry deposition velocities over the ocean during the winter months are likely due to higher wind speeds.

The increased SO_2 dry deposition velocities in UKESM1-SO2 drive an increase in the SO_2 dry deposition burden of nearly 45% (from 29.49 ~~kg~~ T ~~m^{-2}g y^{-1}~~ y^{-1} to 42.56 $Tg\,y^{-1}$) and subsequently reduce the SO_2 lifetime by approximately 25% (see Table C1). Overall the global SO_2 burden is reduced from 0.54 $Tg\,y^{-1}$ to $0.41 SO_2$. The full budget breakdown for SO_2 is given in Appendix C (Table C1). The spatial distribution of these changes is illustrated in Figure 11 which shows that SO_2 dry deposition increases over most regions, with a corresponding decrease in surface SO_2 concentrations. The lower SO_2 burden then drives lower oxidation fluxes (Table C1), reducing the surface SO_4^{2-} concentrations (Figure 11g-i).

The largest absolute increases in SO_2 dry deposition occur over the main source regions of USA–E, eastern China, and central and eastern Europe (Figure 11b). However, Figure 11c shows that the largest relative changes in dry deposition are over the ocean~~, with SO_2 dry deposition increasing up to 100% in the southern ocean. Over other ocean areas, the increase was 20–80%.~~. Although the absolute changes over the ocean are small ($<1\times10^{-5}$ $kg\,m^{-2}\,y^{-1}$), the large global surface area of ocean means that this increase is important for the global sulphur cycle. In UKESM1-SO2 R_{surf}-mod increases the length of time land surfaces remain wet after rainfall, thus increasing SO_2 dry deposition over most land surfaces (as seen in Figures 11b) due to the high solubility of SO_2 in water. Note that R_{surf}-mod also makes SO_2 dry deposition a function of the soil moisture content and this aspect of ~~this~~ the change drives decreases in SO_2 dry deposition of 20-40% over desert regions, such as the Sahara and high northern latitudes (see Figures 11b and c). Conversely R_{surf}-mod does not impact ocean surfaces and the increases in SO_2 dry deposition over oceans ~~seen in Figures 11c~~ are driven by R_{water}-mod.

The largest absolute reductions in mean annual surface SO_2 and SO_4^{2-} concentrations are over the source regions, corresponding with the locations of the largest increases in SO_2 dry deposition. This is expected because dry deposition of SO_2 to the surface is directly proportional to the surface concentration (Equation ~~??~~1). Figure 11e shows that mean annual surface SO_2 concentration was reduced by up to 20 $\mu g\,m^{-3}$ in the eastern USA, eastern China, and central and eastern Europe, which corresponds to a percentage decrease of 30-50%. Note that this is similar to the percentage decrease in mean annual surface SO_2 concentration over remote and ocean regions, although the absolute fluxes are much larger over the source regions. With the exception of some areas in the Sahara and the Middle East, we do not see increases in mean annual surface SO_2 concentration where dry deposition fluxes decrease (albeit by very low amounts), such as the Arctic. We suggest that this is because these areas are remote and contain no SO_2 sources and by reducing SO_2 in the source regions, we reduce overall atmospheric SO_2 loading and therefore less is transported to remote areas. Figures 11h and i show that mean annual surface SO_4^{2-} concentrations are also reduced over the main source regions, although the reductions over the USA are relatively small compared to the other large source regions (0.5 $\mu g\,m^{-3}$ compared with up to 3 $\mu g\,m^{-3}$ in central and eastern Europe and China). Proportionally, the reduction in mean annual surface SO_4^{2-} concentration is smaller than that for mean annual SO_2 concentration, with decreases

28

generally less than 5% over most source regions.

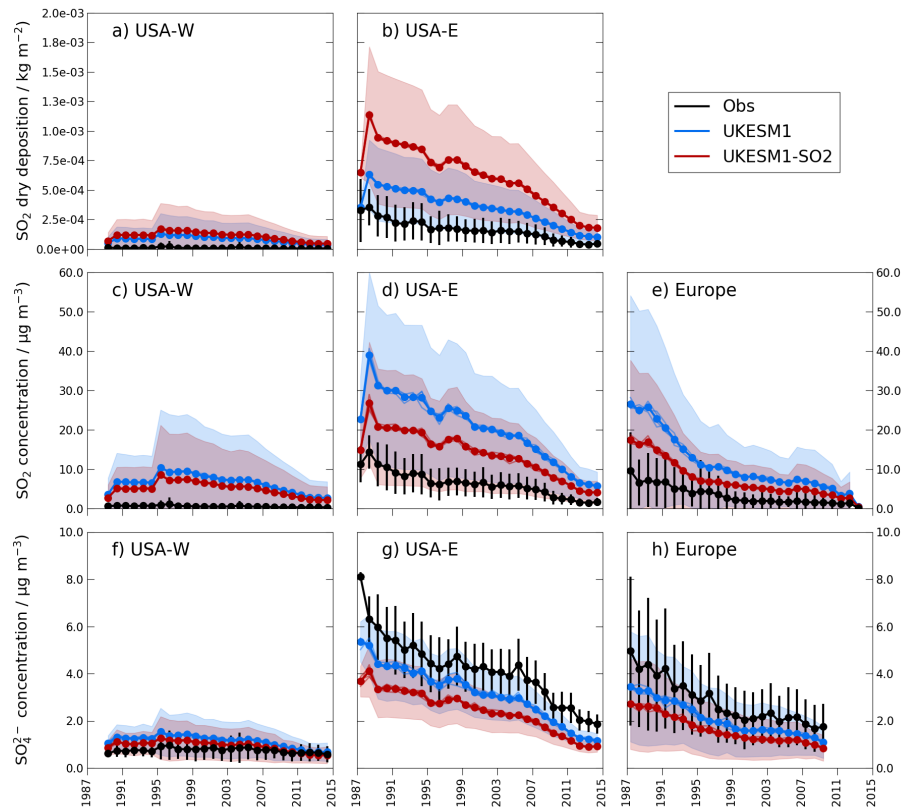## 4.2 Evaluation of UKESM1-SO2 against ground-based observations

Figure 12. Time series of observed and modelled mean annual SO_2 dry deposition flux (top row), surface SO_2 concentration (middle row) and SO_4^{2-} concentration (bottom row) for USA–W, (a, c, f; N sites $= 16$); USA–E, (b, d, g; N sites $= 33$) and Europe (e, h; N SO_2 sites $= 48$ and N SO_4^{2-} sites $= 42$). No SO_2 dry deposition flux observations are available for Europe.

In Figure 12 and Table 7 we evaluate UKESM1-SO2 against the ground-based observations of mean annual surface SO_2 and SO_4^{2-} concentration for the USA and ~~Europe~~ European regions over the period from 1987–2014. UKESM1-SO2 is also evaluated against SO_2 dry deposition flux from CASTNet over the same period. Figures 12 a and b show that SO_2 dry deposition flux is increased in UKESM1-SO2 relative to UKESM1 with this increase being more pronounced over USA–E compared with USA–W (see also Table 7). The increase in SO_2 dry deposition in UKESM1-SO2 does enhance the model's over-prediction of this parameter relative to the CASTNet data, with NMB increasing from 1.15 in UKESM1 to 3.0 in UKESM1-SO2. Mean annual SO_2 dry deposition fluxes are very low over USA–W due to the much lower concentrations of SO_2 in this region.

Table 7. Statistics for mean annual surface SO_2 and SO_4^{2-} concentrations and SO_2 dry deposition flux for UKESM1 and UKESM1-SO2. The mean seasonal values are averaged over the period 1987–2014. The units for SO_2 and SO_4^{2-} concentrations are $\mu g\,m^{-3}$ and the units for dry deposition flux are $kg\,m^{-2}\,y^{-1}$ for SO_2.

	USA–W		USA–E		Europe	
	UKESM1	UKESM1-SO2	UKESM1	UKESM1-SO2	UKESM1	UKESM1-SO2
SO_2 dry deposition						
Mean (obs)	6.11×10^{-6}	-	1.64×10^{-4}	-	-	-
Mean	8.16×10^{-5}	1.17×10^{-4}	3.50×10^{-4}	6.17×10^{-4}	-	-
Bias	7.75×10^{-5}	1.03×10^{-4}	1.87×10^{-4}	4.53×10^{-4}	-	-
NMB	12.41	16.96	1.27	2.98	-	-
N sites	16	-	33	-	-	-
SO_2 concentration						
Mean (obs)	0.48	-	6.34	-	2.94	-
Mean (model)	6.48	5.02	20.50	14.10	10.20	6.60
Bias	6.00	4.54	14.20	7.72	7.26	3.67
NMB	12.54	9.52	2.41	1.34	2.61	1.36
N sites	16	-	33	-	48	-
SO_4^{2-} concentration						
Mean (obs)	0.70	-	3.82	-	2.76	-
Mean	1.15	0.95	3.14	2.42	1.91	1.48
Bias	0.43	0.24	-0.67	-1.39	-0.85	-1.28
NMB	0.72	0.41	-0.19	-0.38	-0.31	-0.47
N sites	16	-	33	-	42	-

UKESM1 does over-predict mean annual SO_2 dry deposition flux in this region too, but the absolute bias changes very little in UKESM1-SO2 (see Table 7). Figures 12 c - e show that model bias in mean annual surface SO_2 concentration is reduced in UKESM1-SO2 compared with UKESM1 in all three regions over the period 1987–2014. The largest absolute reduction is in USA–E where mean annual surface SO_2 concentration decreases from 20.05 $\mu g\,m^{-3}$ to 14.10 $\mu g\,m^{-3}$, however, the largest reduction in NMB is in USA–W where it decreases from 12.54 to 9.52 (see Table 7). The model's over prediction of mean annual surface SO_4^{2-} concentration is reduced over USA–W in UKESM1-SO2 compared with UKESM1, with NMB decreasing from 0.72 to 0.41. However, the model's under prediction of mean annual surface SO_4^{2-} concentration over USA–E and Europe increases, with NMB = -0.31 in UKESM1 and NMB = -0.47 in UKESM1-SO2

(see Table 7). We find that the changes to the surface concentration and dry deposition flux occur almost uniformly over the seasonal cycle and so do not change the patterns in seasonal bias that are described in Section 3.4 for surface SO_2 and SO_4^{2-} concentrations.

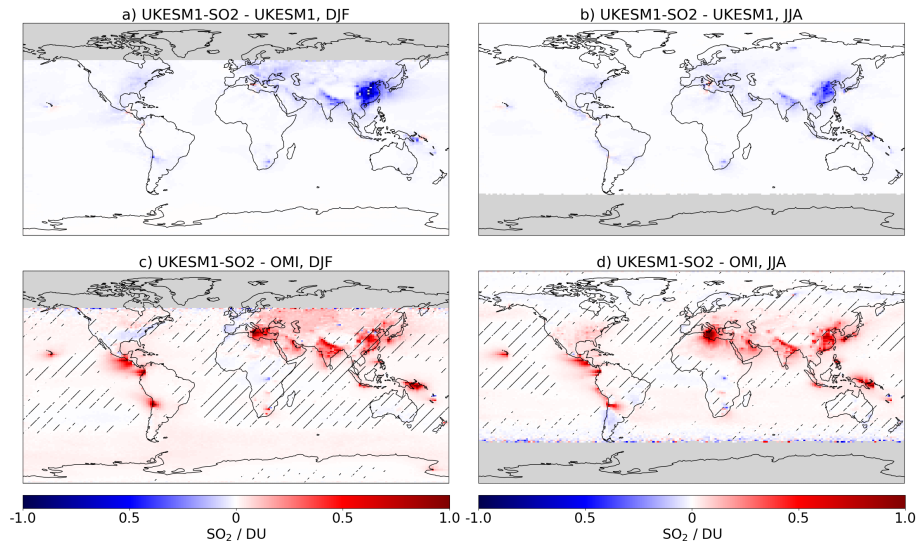## 595   4.3   Evaluation of UKESM1-SO2 against $TCSO_2$ observations

Figure 13. Difference in $TCSO_2$ between UKESM1 and UKESM-SO2 for DJF (a) and JJA (b). Difference in $TCSO_2$ between UKESM1-SO2 and OMI for DJF (c) and JJA (d). Model and satellite data is averaged over the period 2005–2014. The hatched regions show where the inter-model differences are smaller than the existing model-satellite difference

The impact of the modifications to the SO_2 dry deposition parameterization on $TCSO_2$ are shown in Figure 13 and Table 6. Figures 13 a and b show that $TCSO_2$ over the source regions is lower in UKESM1-SO2 relative to UKESM1 by $0.1 - 0.5$ DU in DJF and JJA. This results in UKESM1-SO2 having a smaller positive bias in $TCSO_2$ ~~compared with that of UKESM.~~ ~~Figures 13c and d show that UKESM1-SO2 – OMI is~~ of $+0.3 - +0.5$ DU ~~over source regions compared to~~ compared with that of $+0.6 - +1.0$ DU for UKESM1 ~~– OMI (see Section 3.5 ,~~ (Figures 13c and d; Section 3.5 and Figure 8). This represents a 600   decrease in the global $TCSO_2$ model - OMI bias of 20-30%. Over the outflow regions (e.g. off the USA eastern seaboard), $TCSO_2$ has reduced by 30-50% and over the source regions, this varies by 30-50% for South to North East Asia, 20-30% for Europe and 10-30% for the USA (see Table 6). However, Figures 13c and d also show that the inter-model differences are smaller than the existing model-satellite difference, i.e. the hatched regions are sporadic with limited coverage.

605

31

5 Discussion

The evaluation of UKESM1 against ground-based observations of SO_2 and SO_4^{2-} concentrations from the USA and Europe, as well as SO_2 dry deposition fluxes from the USA, shows that the model is able to represent recent historical changes in these variables. UKESM1 is also able to capture the spatial patterns in surface SO_2 and SO_4^{2-} concentrations and SO_2 dry deposition, simulating larger values close to the sources and lower values away from the sources. However, UKESM1 generally over-predicts surface SO_2 concentrations and dry deposition fluxes, while under-predicting surface SO_4^{2-} concentrations ~~over~~ for the period 1987-2014. Further, we find that UKESM1 over-predicts the rate at which the surface SO_2 concentrations decrease over this period.

We also make use of the updated $TCSO_2$ product from OMI to evaluate UKESM1, finding that the model captures spatial patterns in $TCSO_2$ at the global scale. Importantly, this evaluation allows us to identify model bias in regions without long-term ground-based networks, showing that UKESM1 over-predicts $TCSO_2$ over all source and outflow regions. We find that although the ground-based and satellite observations are subject to different uncertainties, UKESM1's relative over-prediction of both surface SO_2 concentration and $TCSO_2$ is similar in the USA and Europe. This suggests that our ~~findings~~ finding of positive bias in modelled atmospheric SO_2 is robust. We have also demonstrated that a more realistic treatment of SO_2 dry deposition in UKESM1 reduces the model's atmospheric loading of SO_2 and SO_4^{2-}. However, we find that UKESM1's under-prediction of surface SO_4^{2-} concentrations and over-prediction of SO_2 dry deposition fluxes increases when the changes are included in the model, suggesting that there are further uncertainties UKESM1's representation of the complex sulphur cycle processes. Additionally, the spatial and temporal differences in the model bias suggests that the drivers of model bias are regionally and seasonally dependant.

Broadly, ~~model bias in~~ a model's over prediction of atmospheric SO_2 can be driven by too little removal of SO_2 ~~from the atmosphere~~ (via deposition or oxidation) or too high emissions. UKESM1 uses SO_2 emissions from CMIP6 (Eyring et al., 2016). In comparing these emissions with the HTAP-OMI (Liu et al., 2018) and EDGAR (Crippa et al., 2018) data sets, Pope and Chipperfield (2021) showed that the total SO_2 emissions in CMIP6 ($115\,\mathrm{Tg\,y^{-1}}$) are moderately larger than the HTAP-OMI ($100\,\mathrm{Tg\,y^{-1}}$) and EDGAR data sets ~~. Further, comparing the spatial distribution showed that the~~ ($102\,\mathrm{Tg\,y^{-1}}$). In general the CMIP6 emissions ~~from almost all sources are larger than~~ are larger that the HTAP-OMI ~~emissions~~ and EDGAR emissions over all major source regions by up to $1\times10^{-10}\,\mathrm{kg\,m^{-2}\,y^{-1}}$. Exceptions occur at a number of point locations, which are likely from OMI rather than HTAP ~~.~~ (Liu et al., 2018). Additionally, Smith (2021) has reported that SO_2 emissions over the western USA are too high, possibly because the proxy data used to spatially distribute emissions does not take into account lower sulphur coal used in power plants and industry in this region.

Emission injection height is also an important constraint on near surface SO_2 concentrations as demonstrated by Yang et al. (2019). This study found that uncertainty in industrial emission height resulted in modeled near-surface SO_2 concentra-

640 tions varying between 70% and 130% over most land regions, higher than the overall uncertainty of 8-14% attributed to SO_2 emission rates. The SO_2 injection height in UKESM1 was investigated by Mulcahy et al. (2020) who used injection heights prescribed as for HadGEM-GC3.1, where 50% of energy and industry sector emissions are injected in to the atmosphere at a height of 500 m. Mulcahy et al. (2020) showed that the introduction of a vertical profile for SO_2 emissions in UKESM1 had negligible impact on surface SO_4^{2-} concentrations at measurement sites in Europe and the USA, suggesting an important role

645 for the aerosol chemistry in these regions. Emitting the SO_2 at higher altitudes will act to reduce surface SO_2 concentrations and therefore model's bias against surface observations of both SO_2 concentration and SO_2 dry deposition flux. However, Pope and Chipperfield (2021) showed that ~~model~~ UKESM1's bias in TCSO_2 increased when emission injection heights were increased. This ~~finding further~~ also suggests that the CMIP6 emissions are too high and that using a vertical profile for the emissions to some extent shifts the model's bias in SO_2 to higher altitudes. However, we note that using varying emission heights

650 for SO_2 did not affect column densities in the GEOS-5/GOCART model (Buchard et al., 2014). We suggest that undertaking model experiments with different emissions inventories and injection height profiles ~~should be able to cast some~~ to cast light on the role of SO_2 emissions in model bias in the sulphur cycle.

The two main removal pathways for SO_2 are oxidation to sulphate and dry deposition to the Earth's surface. In this study

655 we have evaluated a more realistic treatment of SO_2 dry deposition in UKESM1 that accounts for the high solubility of SO_2 in water~~, finding that it reduces the models' atmospheric loading of~~. We find that this reduces the dry deposition lifetime and consequently reduces the overall SO_2 burden and lifetime. This reduces positive model bias in surface SO_2 concentrations in the USA and Europe, and in TCSO_2 across most of the globe. The changes have the largest impact over source regions because dry deposition flux is directly proportional to the atmospheric concentration of SO_2 ~~(Equation ??). However, while~~

660 ~~we see a direct reduction in UKESM1's bias in atmospheric~~. There is also a reduction in the SO_2 ~~loading~~ oxidation lifetime which likely drives the reduced atmospheric loading of SO_4^{2-}. However, the true impact of the changes to the dry deposition parameterization are confounded by model uncertainty in other aspects of the complex sulphur cycle as well as the inherent difficulties associated with evaluating a global model against point observations.

665 Dry deposition is a highly parameterized process and often poorly represented, particularly in global models. Similarly to UKESM1, Vet et al. (2014) showed that SO_2 dry deposition fluxes were over-predicted by the 23 member model ensemble used for the TF-HTAP exercise relative to inferential data sets from measurement networks (including CASTNet). A key uncertainty highlighted in this study was that associated with the inferred dry deposition fluxes; from CASTNet these could be up to 30% lower than direct observations of SO_2 dry deposition flux (Baumgardner et al., 2002). However, the fluxes simulated

670 by UKESM1 are a factor of 2 to 10 higher than the inferred data from USA–E and USA–W, indicating that the modelled deposition fluxes are almost certainly too large. Additional sources of uncertainty in model simulations of SO_2 dry deposition may include land surface cover, changes in the atmospheric $SO_2:NH_3$ ratio and the ratio between wet and dry deposition of SO_2. Mulcahy et al. (2020) showed that wet deposition, and to a lesser extent dry deposition, of SO_2 was considerably lower in UKESM1 compared with HadGEM-GC3.1. Paulot et al. (2017) also report that poor representation of wet deposition likely

contributed to bias in modelled surface SO_4^{2-} concentrations. Too low wet deposition would also contribute to the model's over-prediction of surface SO_2 concentration. Dry deposition is sensitive to land surface type, which may not be well captured in global models. In this study the UKESM1 configuration uses 13 land cover classes including 11 plant functional types (Archibald et al., 2020). This is reasonable for a global model, but inevitably detail is lost. Vet et al. (2014) also suggest that SO_2 dry deposition may depend on the atmospheric NH_3 loading. Long term measurements at a UK site showed that SO_2 dry deposition velocity has increased with time, which was attributed to changing ratios of SO_2:NH_3 as SO_2 concentrations have decreased faster than NH_3 concentrations (Vet et al., 2014; Fowler et al., 2009). Currently nitrate chemistry is not represented in UKESM1, although it is planned for future model versions, and NH_3 has not been evaluated in the model, so it is unknown how these factors may contribute to the model's bias in SO_2 dry deposition flux and SO_2 concentrations.

The role of uncertainty in sulphur cycle chemistry becomes apparent when we consider UKESM1's bias in surface SO_4^{2-} concentrations in combination with the biases in SO_2 concentrations and dry deposition. In Europe and USA–E, UKESM1 under-predicts surface SO_4^{2-} concentrations, despite the large positive biases in SO_2 concentrations through much of the period from 1987-2014. Note that there are exceptions close to certain point sources, particularly in Europe. However, in the cleaner USA–W region surface SO_4^{2-} concentrations are consistently over-predicted. We suggest that in USA–W too high SO_2 emissions (Smith, 2021), possibly in combination with too low emission heights and the associated biases in dry deposition, drive the model's over-prediction of surface SO_4^{2-} concentrations in this region. However, ~~In~~ in the polluted regions of Europe and USA–E the under-prediction of surface SO_4^{2-} concentrations, despite large over-predictions of surface SO_2 concentrations suggests that sulphur cycle chemistry is not correctly represented~~there. In addition, UKESM1 is known to under-predict surface O_3 concentrations (Archibald et al., 2020).~~. And Mulcahy et al. (2020) showed that there are global and regional differences in oxidant concentrations and in the SO_2 lifetime between UKESM1 and the ~~HadGEMGC3~~HadGEM-GC3.1 model, with the latter better able to capture surface SO_4^{2-} concentrations. In reducing the SO_2 burden we further reduce its overall lifetime and oxidation lifetime relative to HadGEM-GC3.1. This highlights the requirement for a more detailed investigation of SO_2 oxidation in UKESM1, particularly in polluted regions.

~~Further, uncertainty~~ Uncertainty in UKESM1's sulphur chemistry also appears to be seasonally dependant. In USA–E and Europe UKESM1 over-predicts SO_2 (surface concentration and $TCSO_2$) and under-predicts surface SO_4^{2-} at all times of the year, but there is seasonal variation in these biases. In Europe, the model bias is largest in DJF which drives a stronger seasonal cycle relative to the observations. This is in agreement with Turnock et al. (2015) who investigated SO_4^{2-} in an earlier HadGEM3-UKCA configuration. The seasonality in UKESM1's bias over Europe may be due to the model under-predicting in-cloud SO_2 oxidation via O_3 (Table 1). In winter and at higher latitudes this reaction is likely to be the dominant removal pathway due to lower availability of H_2O_2 (Turnock et al., 2019). However, the picture is different in USA–E, where UKESM1 over-predicts SO_2 to a larger extent in JJA compared with DJF and there is little seasonality in the model's under-prediction SO_4^{2-}. In USA–E it is likely that uncertainty in UKESM1's representation of SO_2 oxidation via both O_3 and H_2O_2 (Table 1) ~~contributes to the~~ contribute to bias in SO_2 and SO_4^{2-} ~~as the higher~~. The lower average latitude of the

710   USA–E sites ~~mean~~ compared with European sites, means that the O_3 oxidation pathway is ~~less~~ more important in this region and ~~Paulot et al. (2017) showed~~ it has been demonstrated that SO_4^{2-} concentrations are sensitive to both pathways in winter Paulot et al. (2017). From this study it is not clear what is driving the relatively large positive bias in SO_2 in JJA over USA–E and we stress the need for closer examination of the sulphur chemistry in UKESM1.

715   Recent studies have also shown that cloud water pH may be an important factor in the aqueous phase oxidation of SO_2 to SO_4^{2-} (Turnock et al., 2019). While a temporally and spatially uniform cloud pH of 5 is currently used in UKESM1, observations of this quantity show that it varies in space and time. Observations at an American site showed that mean cloud pH increased from 4 to 4.8 between 1994 and 2014 (Schwab et al., 2016)~~; at~~, cloud pH measured Mt Tai in North China ~~values of cloud pH measured in~~ from 2007-2008 were between 3.56 and 7.64, and measurement campaigns between 1985

720 and 2008 at various European, North American and East Asian locations reported values between 3.34 and 5.29 (Guo et al., 2012). Turnock et al. (2019) showed that varying this value in the HadGEM3-UKCA model can have a large impact on SO_2 and SO_4^{2-} concentrations. Over source regions, including Europe and North America, increasing the cloud water pH by 1.0 reduced the annual mean global SO_2 column burden by approximately 50% as more SO_2 was oxidized in cloud droplets, and consequently there were small increases in the annual mean sulphate column burden over these regions. Conversely, outside

725 of polluted regions increasing the cloud water pH reduced the sulphate column burden by 10% to 40% globally. These results indicate that having a more realistic treatment of cloud water pH could reduce UKESM1's biases in $TCSO_2$, and potentially in SO_2 and SO_4^{2-} concentrations remote from source regions. However, is unlikely to be a dominant removal pathway at the surface and any impact on surface SO_2 concentrations, especially close to sources would ~~be expected to be~~ likely be minimal.

730   In an Earth system model such as UKESM1, there are inevitably some compromises in the complexity of the chemistry and aerosol scheme as these are computationally expensive. While the sulphur chemistry represented in the UKCA-StratTrop model used in UKESM1 accounts for important SO_2 and DMS oxidation reactions, as well as simulating oxidants (rather than the offline oxidant scheme used in HadGEM-GC3.1) it cannot be complete. In the recently developed CRI-Strat scheme the sulphur chemistry reactions are as for ~~UKCA-STratTrop~~UKCA-StratTrop, but there is a more comprehensive treatment of

735 non-methane volatile compounds (NMVOC) (Archer-Nicholls et al., 2020) resulting in higher surface ozone concentrations, particularly over polluted areas in summer, compared with UKCA-StratTrop. As demonstrated by Mulcahy et al. (2020) the increased oxidants in UKESM1 relative to HadGEM-GC3.1 likely contribute to reducing the SO_2 lifetime from 4.29 to 3.86 days. CRI-Strat is ~~able to be used in~~ compatible with UKESM1 and the higher oxidant loading may reduce SO_2 oxidation lifetime further with a concurrent increase in SO_4^{2-}. ~~The impact of more detailed DMS oxidation chemistry~~ Model bias in

740 remote ocean regions may also result from the necessarily simplified DMS oxidation chemistry in UKESM1. A more detailed representation of DMS chemistry over the Southern Ocean was investigated by Revell et al. (2019) who found that surface SO_2 concentrations increased over the Southern Ocean, possibly due to including reactions ~~of DMS with halogen species. Revell et al. (2019) also found that~~ between DMS and halogen species, while SO_4^{2-} concentrations decreased, likely as a result of there being more DMS oxidation reactions. ~~Although Revell et al. (2019)'s results focused on the Southern Ocean, the~~

745 ~~global impact of using more complex DMS chemistry would be very informative.~~

Model resolution is also likely to be an important source of model bias in this study. In evaluating UKESM1 against the CASTNet and EMEP data sets we are comparing a simulated value generated from a model grid box ~~approximately~~ at a scale of $\approx$ 200-300 km with a point observation. This may be a particular problem for the surface SO_2 concentrations and

750 SO_2 dry deposition fluxes because in reality a large fraction (20-40%) of SO_2 emitted from point sources is lost in the first 100 km, which is sub-grid scale relative to the model grid boxes (Smith and Jeffrey, 1975; Wys et al., 1978). In UKESM1 ~~all the~~ the sub-grid scale loss is not captured because SO_2 is evenly emitted across the grid box and ~~then the deposition is calculated. In reality in large fraction of the emitted SO_2 never makes it to the grid scale, driving~~ deposition is subsequently calculated. Potentially this drives overall large model biases compared with ~~the~~ ground based observations ~~which~~ that are not

755 necessarily close to the point sources. In addition, the model resolution can not capture complex orography, meaning that transport of SO_2 may not be well represented. This could be ~~a particular problem~~ problematic in mountainous areas of USA–W ~~VanCuren and Gustin (2015)~~(VanCuren and Gustin, 2015). High resolution model studies would be beneficial to address the both importance of orography and to investigate the SO_2 losses close to sources. We also suggest that evaluating UKESM1 against chemical re-analysis fields of SO_2 could reduce some of the bias that occurs with using ~~using~~ point observations, but

760 there are uncertainties associated with this approach too (Ukhov et al., 2020).

6 Conclusions

We evaluate UKESM1 against ground-based and satellite observations of selected sulphur species over the recent historical period. We find that UKESM1 is able to capture the temporal and spatial patterns in surface SO_2, surface sulphate concen-

765 tration, SO_2 dry deposition and $TCSO_2$. However, compared to observations we find that the model is biased, depending on the variable, region and species. We address one possible source of bias by introducing a more realistic treatment of SO_2 dry deposition, a key loss process for this species. This change reduces model bias in surface SO_2 concentrations and $TCSO_2$. However, it is apparent that other biases exits within the complex sulphur cycle and we highlight some key areas for further investigation to better understand these and target areas for development.

770

Our evaluation suggests uncertainty in UKESM1's sulphur chemistry is also an important driver of the biases seen in this study, ~~in particular~~ particularly over polluted regions. Two priorities for further investigation into the oxidation of SO_2 in UKESM1 are (i) an evaluation of the CRI-Strat scheme and (ii) a more realistic treatment of cloud water pH. The model's necessarily limited DMS chemistry may also contribute to bias in atmospheric sulphur loading over remote ocean areas. ~~While~~

775 ~~testing the available, more detailed representations of DMS chemistry in the fully coupled UKESM1 model may not be feasible, their impact at the global scale could be assessed in UKCA.~~ The impact of the nitrate scheme currently in development for UKESM1 will also be investigated in relation to the sulphur cycle. Another ~~aspects~~ aspect of UKESM1's sulphur cycle that

would benefit from more detailed analysis is the ratio between wet and dry deposition and how this compares with observations. We also suggest that high resolution studies to investigate SO_2 deposition close to sources would be beneficial for a better
780   understanding of these processes. Finally, we suggest that the SO_2 emissions may be too high through a possible combination of too high emissions in the CMIP6 inventory and injection of the emissions into the surface layer only.

The sulphur cycle is a key area of analysis and development for UKESM1 given its importance as a driver of historical aerosol forcing. UKESM1 is relatively unique amongst models in CMIP6 in that it has a fully interactive atmospheric chemistry scheme
785   coupled to a two-moment (mass and number) aerosol scheme. Given the complexity of the model's chemistry-aerosol treatment within the ES framework, the model's performance here is encouraging and provides confidence in UKESM1, particularly in regard to capturing the historical trend. However there is always space for improvement and to the more realistic treatment of SO_2 dry deposition will therefore be incorporated into the planned release of UKESM1.1. This latest model version will be documented in an forthcoming publication which will also address the impact of the SO_2 dry deposition changes on aerosol
790   loading and climate.

Code availability. The UM is the source code for the atmosphere-land–ocean–sea ice components of the UKESM1 physical model, including the NEMO and CICE modules for oceans and sea ice, respectively. The UM source code base also houses the GLOMAP-Mode and UKCA modules. JULES is the source code for land and terrestrial biogeochemistry components. MEDUSA is the source code for the
795   ocean biogeochemistry. Due to intellectual property rights restrictions, we cannot provide either the source code or documentation papers for the UM or JULES. *Obtaining the UM.* The Met Office Unified Model is available for use under licence. A number of research organisations and national meteorological services use the UM in collaboration with the Met Office to undertake basic atmospheric process research, produce forecasts, develop the UM code and build and evaluate Earth system models. For further information on how to apply for a licence, see http://www.metoffice.gov.uk/research/modelling-systems/unified-model (last access: 17 March 2021). *Obtaining JULES.*
800   JULES is available under licence, free of charge. For further information on how to gain permission to use JULES for research purposes, see http://jules-lsm.github.io/access_req/JULE_access.html (last access: 17 March 2021). Information about the UKESM1 release and its components and the prerequisites for using it can be found here: http://cms.ncas.ac.uk/wiki/UM/Configurations/UKESM. Briefly, UKESM1 is distributed and run as a Rose suite on the Archer2 and Monsoon computing platforms administered by UK Research Innovation (UKRI) and the Met Office/Natural Environment Research Council (NERC), respectively. Rose is a framework for developing and running meteorological
805   applications and is described in more detail here: http://cms.ncas.ac.uk/wiki/RoseCylc.

Data availability. The simulation data used in this study are archived on the Earth System Grid Federation (ESGF) node (https://esgf-node.llnl.gov/projects/cmip6/, last access: 17 March 2021). The model source ID is UKESM1-0-LL for UKESM1. UKESM1 historical simulations are identified by the following variant labels: r1i1p1f2, r2i1p1f2, r8i1p1f2 and r9i1p1f2, (https://doi.org/10.22033/ESGF/CMIP6.6113; Tang (2019)). We acknowledge the use of the CASTNet data base (https://www.epa.gov/castnet, last access: 17 March 2021). Information on

810 the EMEP network can be found in Tørseth et al. (2012) and the data is available from http://ebas.nilu.no/. OMI total column SO2 data was obtained from NASA's Goddard Earth Sciences Data and Information Services Center (GES DISC, https://disc.gsfc.nasa.gov/, last access: 17 March 2021).

Appendix A: ~~Appendix A~~

Here we describe in detail the changes to UKESM1's parameterization of dry deposition of SO_2 to the surface. These
815 modifications account for the impact of surface wetness due to rainfall or humidity on SO_2 dry deposition to vegetated or soil surfaces. We first derive a parameter, $zwet$ that designates whether a model grid box at time step N is wet or dry. We assume that on entering time step N the grid box in question has a dry surface ($zwet = 0$). If, during time step N, precipitation is greater than a threshold value (set to $0.5\,\mathrm{mm\,day^{-1}}$) the grid box then becomes classed as wet ($zwet = 1$). Once precipitation stops, the grid box is assumed to dry out over a specified period. Assuming no precipitation falls during this drying period, at
820 the end of the period the grid box will be classed as dry ($zwet = 0$). If, during the drying period, a new precipitation event occurs at the grid box, of intensity greater than $0.5\,\mathrm{mm\,day^{-1}}$, $zwet$ is reset to 1. If the precipitation event is less than $0.5\,\mathrm{mm\,day^{-1}}$ but greater than $0.0\,\mathrm{mm\,day^{-1}}$, $zwet$ is not reset to 1 and neither is it decreased in value (i.e. no drying is assumed to occur over that time step). A grid box is classed as wet whenever $zwet > 0$. We tested a range of time periods from three hours to one day and found only minor sensitivity to this parameter. For UKESM1-SO2 we used a drying period of three hours. In future work
825 we will investigate making this parameter a function of surface evaporation and downwelling solar radiation.

If a grid box is classed as wet then R_{soil} and R_{cut} (for all vegetation types) is set equal to $1\,\mathrm{s\,m^{-1}}$. Through Equation 5, R_c will then tend towards a value of $1\,\mathrm{s\,m^{-1}}$, equating to minimal resistance to SO_2 deposition. In these situations, the amount of SO_2 deposited will primarily be limited by the efficiency of gas transport to the receptor surface, i.e. by R_a and R_b in
830 Equation. 2. If the grid box is classed as dry, R_{cut} is calculated following Equation 9 in Erisman et al. (1994), whereby R_{cut} is a decreasing function of near surface relative humidity. If a grid box surface temperature lies between -1°C and -5°C, R_{cut} is reset to $200\,\mathrm{s\,m^{-1}}$ and below -5°C to $500\,\mathrm{s\,m^{-1}}$, irrespective of the near surface relative humidity. For dry grid boxes, R_{soil} uses a value of $213.5\,\mathrm{s\,m^{-1}}$ for all surface temperatures (see Table A2). For dry surfaces, R_{cut} also approaches a value of $1\,\mathrm{s\,m^{-1}}$ as near surface relative humidity approaches a value of one. As for a wet surface, in these conditions there is minimal
835 resistance to SO_2 deposition and R_c will tend towards $1\,\mathrm{s\,m^{-1}}$. Thus SO_2 dry deposition will primarily be limited by R_a and R_b.

Table A1. Summary of the representation of R_{cut} and R_{soil} in UKESM1 and UKESM1-SO2. Units for resistance values are $s\,m^{-1}$

Grid box condition	Surface temperature	Near surface relative humidity (RH)	UKESM1		UKESM1-SO2	
			R_{soil}	R_{cut}	R_{soil}	R_{cut}
Wet	N/A	N/A	213.5	R_{surf}[*]	1.0	1.0
Dry	$>$ -1°C	RH < 0.813	213.5	R_{surf}	213.5	R_{cut}=2.5×10^{-4} exp $[-6.93*RH]$[*]
	$>$ -1°C	RH > 0.813	213.5	R_{surf}	213.5	R_{cut}=0.58×10^{12} exp $[-27.8*RH]$[**]
Dry	$>$ -5°C and $<$ -1°C	N/A	213.5	R_{surf}	213.5	200.0[***]
Dry	$<$ -5°C	N/A	213.5	R_{surf}	213.5	500.0[(***)]

[*] See values in Table A2; [**] Following Erisman et al. (1994); [***] Irrespective of near surface relative humidity

Table A2. Standard surface resistance (R_{surf}) values for SO_2 for land use types in UKESM1. These values were calculated based on the data published in Zhang et al. (2003) for SO_2.

Land surface type	R_{surf} / $s\,m^{-1}$
Broad leaf deciduous	137.0
Broad leaf evergreen tropical	111.1
Broad leaf evergreen temperate	111.9
Needle leaf deciduous	131.3
Needle leaf evergreen	130.4
C3 grass	209.8
C3 crop	30.0
C3 pasture	209.8
C4 grass	196.1
C4 crop	30.0
C4 pasture	196.1
Shrub deciduous	185.8
Shrub evergreen	196.1
Urban	180.7
Water	1.0
Soil	213.5
Ice	215.1

Appendix B
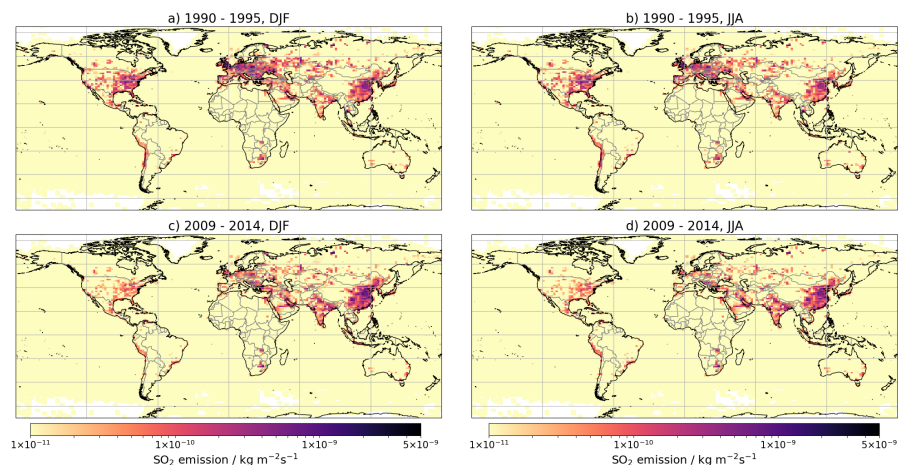
Figure B1. Global emissions of SO_2 used in UKESM1. Mean seasonal emissions are shown for the 1990–1995 time slice for DJF (a) and JJA (b), and the 2009–2014 time slice for DJF (c) and JJA (d).

B1

Appendix C

Table C1. Global SO_2 budget for UKESM1 and UKESM1-SO2. Units for production and loss fluxes are in Tg $[S]\,yr^{-1}$, burdens are in Tg and lifetimes are in days. The values are calculated from a 2 year AMIP simulation covering the period 1981–1983 inclusive.

	UKESM1	UKESM1-SO2
Emission sources		
Surface emission	61.03	61.03
High-level emission	0	0
Natural emission	14.02	14.02
Sources from DMS oxidation		
$DMS + OH \rightarrow SO_2$	6.42	6.37
$DMS + OH \rightarrow SO_2 + MSA$	6.36	-
$DMS + OH \rightarrow 0.6SO_2 + 0.4DMSO$	-	3.83
$DMS + NO_3 \rightarrow SO_2$	3.48	3.47
$DMSO + OH \rightarrow 0.6SO_2$	-	1.53
$DMS + O(^3P) \rightarrow SO_2$	0.1708	0.1738
Sources from COS oxidation		
$COS + O(^3P) \rightarrow CO + SO_2$	7.92×10^{-3}	7.87×10^{-3}
$COS + OH \rightarrow CO_2 + SO_2$	0.105	0.106
$COS + hv \rightarrow CO + SO_2$	0.024	0.0235
Losses from gas-phase oxidation		
$SO_2 + OH \rightarrow SO_3 + HO_2$	18.66	14.86
$SO_2 + O_3 \rightarrow SO_3$	8.19×10^{-4}	6.54×10^{-4}
$SO_3 + H_20 \rightarrow H_2SO_4 + H_2O$		
$SO_3 + hv \rightarrow SO_2 + O(^3P)$	4.07×10^{-9}	4.46×10^{-9}
Losses from aqueous-phase oxidation		
$HSO_3 + H_2O_2 \rightarrow SO_4$	20.52	16.46
$HSO_3 + O_3 \rightarrow SO_4$	0.2372	0.1625
$SO_3 + O_3 \rightarrow SO_4$	9.22	6.35
Dry Deposition	29.49	42.56
Wet Deposition	14.09	10.57
Total Sources	91.62	90.56
Total Losses	92.22	90.96
Burden	0.54	0.41
Lifetime	2.11	1.62
Oxidation lifetime	3.997	3.901
Dry deposition lifetime	6.59	3.47
Wet deposition lifetime	13.80	13.96

REFERENCE 1
REFERENCE 2

References

Aas, W., Mortier, A., Bowersox, V., Cherian, R., Faluvegi, G., Fagerli, H., Hand, J., Klimont, Z., Galy-Lacaux, C., Lehmann, C. M. B., Myhre, C. L., Myhre, G., Olivie, D., Sato, K., Quaas, J., Rao, P. S. P., Schulz, M., Shindell, D., Skeie, R. B., Stein, A., Takemura, T., Tsyro, S., Vet, R., and Xu, X.: Global and regional trends of atmospheric sulfur, SCIENTIFIC REPORTS, 9, https://doi.org/10.1038/s41598-018-37304-0, 2019.

Aleksic, N., Roy, K., Sistla, G., Dukett, J., Houck, N., and Casson, P.: Analysis of cloud and precipitation chemistry at Whiteface Mountain, NY, Atmospheric Environment, 43, 2709–2716, 2009.

Altshuller, A.: Model predictions of the rates of homogeneous oxidation of sulfur dioxide to sulfate in the troposphere, Atmospheric Environment (1967), 13, 1653 – 1661, https://doi.org/https://doi.org/10.1016/0004-6981(79)90323-8, http://www.sciencedirect.com/science/article/pii/0004698179903238, 1979.

Archer-Nicholls, S., Abraham, N. L., Shin, Y. M., Weber, J., Russo, M. R., Lowe, D., Utembe, S., O'Connor, F. M., Kerridge, B., Latter, B., et al.: The Common Representative Intermediates Mechanism version 2 in the United Kingdom Chemistry and Aerosols Model, Earth and Space Science Open Archive ESSOAr, 2020.

Archibald, A. T., O'Connor, F. M., Abraham, N. L., Archer-Nicholls, S., Chipperfield, M. P., Dalvi, M., Folberth, G. A., Dennison, F., Dhomse, S. S., Griffiths, P. T., Hardacre, C., Hewitt, A. J., Hill, R. S., Johnson, C. E., Keeble, J., Köhler, M. O., Morgenstern, O., Mulcahy, J. P., Ordóñez, C., Pope, R. J., Rumbold, S. T., Russo, M. R., Savage, N. H., Sellar, A., Stringer, M., Turnock, S. T., Wild, O., and Zeng, G.: Description and evaluation of the UKCA stratosphere–troposphere chemistry scheme (StratTrop vn 1.0) implemented in UKESM1, Geoscientific Model Development, 13, 1223–1266, https://doi.org/10.5194/gmd-13-1223-2020, https://gmd.copernicus.org/articles/13/1223/2020/, 2020.

Baldocchi, D. D., Hicks, B. B., and Camara, P.: A canopy stomatal resistance model for gaseous deposition to vegetated surfaces, Atmospheric Environment (1967), 21, 91–101, 1987.

Baumgardner, R., Lavery, T., Rogers, C., and Isil, S.: Estimates of the atmospheric deposition of sulfur and nitrogen species: Clean Air Status and Trends Network, 1990-2000, ENVIRONMENTAL SCIENCE & TECHNOLOGY, 36, 2614–2629, https://doi.org/10.1021/es011146g, 2002.

Best, M. J., Pryor, M., Clark, D. B., Rooney, G. G., Esser y, R. L. H., Ménard, C. B., Edwards, J. M., Hendry, M. A., Porson, A., Gedney, N., Mercado, L. M., Sitch, S., Blyth, E., Boucher, O. ., Cox, P. M., Grimmond, C. S. B., and Harding, R. J.: The Joint UK Land Environment Simulator (JULES), model description – Par t 1: Energy and water fluxes, Geoscientific Model Development, 4, 677–699, https://doi.org/10.5194/gmd-4-677-2011, https://gmd.copernicus.org/articles/4/677/2011/, 2011.

Boucher, O., Randall, D., Artaxo, P., Bretherton, C., Feingold, G., Forster, P., Kerminen, V.-M., Kondo, Y., Liao, H., Lohmann, U., et al.: Clouds and aerosols, in: Climate change 2013: the physical science basis. Contribution of Working Group I to the Fifth Assessment Report of the Intergovernmental Panel on Climate Change, pp. 571–657, Cambridge University Press, 2013.

Buchard, V., da Silva, A. M., Colarco, P., Krotkov, N., Dickerson, R. R., Stehr, J. W., Mount, G., Spinei, E., Arkinson, H. L., and He, H.: Evaluation of GEOS-5 sulfur dioxide simulations during the Frostburg, MD 2010 field campaign, Atmospheric Chemistry and Physics, 14, 1929–1941, https://doi.org/10.5194/acp-14-1929-2014, https://acp.copernicus.org/articles/14/1929/2014/, 2014.

Chin, M., Rood, R. B., Lin, S.-J., M??ller, J.-F., and Thompson, A. M.: Atmospheric sulfur cycle simulated in the global model GOCART: Model description and global properties, Journal of Geophysical Research: Atmospheres, 105, 24 671–24 687, https://doi.org/https://doi.org/10.1029/2000JD900384, https://agupubs.onlinelibrary.wiley.com/doi/abs/10.1029/2000JD900384, 2000.

Clark, D. B., Mercado, L. M., Sitch, S., Jones, C. D., Ged ney, N., Best, M. J., Pryor, M., Rooney, G. G., Essery, R. L. H., Blyth, E.,

905   Boucher, O., Harding, R. J., Huntingford, C., and Cox, P. M.: The Joint UK Land Environment Simulator (JULES), model description –
        Par t 2: Carbon fluxes and vegetation dynamics, Geoscientific Model Development, 4, 701–722, https://doi.org/10.5194/gmd-4-701-2011,
        https://gmd.copernicus.org/articles/4/701/2011/, 2011.

Clarke, J., Edgerton, E., and Martin, B.: Dry deposition calculations for the clean air status and trends network, ATMOSPHERIC ENVI-
        RONMENT, 31, 3667–3678, https://doi.org/10.1016/S1352-2310(97)00141-6, 1997.

910 Crippa, M., Guizzardi, D., Muntean, M., Schaaf, E., Dentener, F., van Aardenne, J. A., Monni, S., Doering, U., Olivier, J. G. J., Pagliari,
        V., and Janssens-Maenhout, G.: Gridded emissions of air pollutants for the period 1970-2012 within EDGAR v4.3.2, EARTH SYSTEM
        SCIENCE DATA, 10, 1987–2013, https://doi.org/10.5194/essd-10-1987-2018, 2018.

Dentener, F., Kinne, S., Bond, T., Boucher, O., Cofala, J., Generoso, S., Ginoux, P., Gong, S., Hoelzemann, J. J., Ito, A., Marelli, L., Penner,
        J. E., Putaud, J.-P., Textor, C., Schulz, M., van der Werf, G. R., and Wilson, J.: Emissions of primary aerosol and precursor gases in the

915   years 2000 and 1750 prescribed data-sets for AeroCom, Atmospheric Chemistry and Physics, 6, 4321–4344, https://doi.org/10.5194/acp-
        6-4321-2006, https://acp.copernicus.org/articles/6/4321/2006/, 2006.

Dyer, A.: A review of flux-profile relationships, Boundary-Layer Meteorology, 7, 363–372, 1974.

E. Sickles, II, J. and Shadwick, D. S.: Changes in air quality and atmospheric deposition in the eastern United States: 1990-2004, JOURNAL
        OF GEOPHYSICAL RESEARCH-ATMOSPHERES, 112, https://doi.org/10.1029/2006JD007843, 2007.

920 Erisman, J. W. and Baldocchi, D.: Modelling dry deposition of SO2, Tellus B, 46, 159–171, https://doi.org/https://doi.org/10.1034/j.1600-
        0889.1994.t01-2-00001.x, https://onlinelibrary.wiley.com/doi/abs/10.1034/j.1600-2-00001.x, 1994.

Erisman, J. W., Pul, A. V., and Wyers, P.: Parametrization of surface resistance for the quantification of atmospheric deposition of acidifying
        pollutants and ozone, Atmospheric Environment, 28, 2595 – 2607, https://doi.org/https://doi.org/10.1016/1352-2310(94)90433-2, http:
        //www.sciencedirect.com/science/article/pii/1352231094904332, 1994.

925 Eyring, V., Bony, S., Meehl, G. A., Senior, C. A., Stevens, B., Stouffer, R. J., and Taylor, K. E.: Overview of the Coupled Model Intercom-
        parison Project Phase 6 (CMIP6) experimental design and organization, GEOSCIENTIFIC MODEL DEVELOPMENT, 9, 1937–1958,
        https://doi.org/10.5194/gmd-9-1937-2016, 2016.

Feng, L., Smith, S. J., Braun, C., Crippa, M., Gidden, M. J., Hoesly, R., Klimont, Z., van Marle, M., van den Berg, M., and van der Werf,
        G. R.: The generation of gridded emissions data for CMIP6, Geoscientific Model Development, 13, 461–482, https://doi.org/10.5194/gmd-

930   13-461-2020, https://gmd.copernicus.org/articles/13/461/2020/, 2020.

Finkelstein, P., Ellestad, T., Clarke, J., Meyers, T., Schwede, D., Hebert, E., and Neal, J.: Ozone and sulfur dioxide dry deposition
        to forests: Observations and model evaluation, JOURNAL OF GEOPHYSICAL RESEARCH-ATMOSPHERES, 105, 15 365–15 377,
        https://doi.org/10.1029/2000JD900185, 2000.

Fioletov, V. E., McLinden, C. A., Krotkov, N., Li, C., Joiner, J., Theys, N., Carn, S., and Moran, M. D.: A global catalogue of large

935   SO2 sources and emissions derived from the Ozone Monitoring Instrument, Atmospheric Chemistry and Physics, 16, 11 497–11 519,
        https://doi.org/10.5194/acp-16-11497-2016, https://acp.copernicus.org/articles/16/11497/2016/, 2016.

Fowler, D.: DRY DEPOSITION OF SO2 ON AGRICULTURAL CROPS, in: Sulfur in the Atmosphere, edited by HUSAR, R.,
        LODGE, J., and MOORE, D., pp. 369 – 373, Pergamon, https://doi.org/https://doi.org/10.1016/B978-0-08-022932-4.50041-0, http:
        //www.sciencedirect.com/science/article/pii/B9780080229324500410, 1978.

940 Fowler, D., Pilegaard, K., Sutton, M. A., Ambus, P., Raivonen, M., Duyzer, J., Simpson, D., Fagerli, H., Fuzzi, S., Schjoerring, J. K.,
        Granier, C., Neftel, A., Isaksen, I. S. A., Laj, P., Maione, M., Monks, P. S., Burkhardt, J., Daemmgen, U., Neirynck, J., Personne, E.,

Wichink-Kruit, R., Butterbach-Bahl, K., Flechard, C., Tuovinen, J. P., Coyle, M., Gerosa, G., Loubet, B., Altimir, N., Gruenhage, L., Ammann, C., Cieslik, S., Paoletti, E., Mikkelsen, T. N., Ro-Poulsen, H., Cellier, P., Cape, J. N., Horvath, L., Loreto, F., Niinemets, U., Palmer, P. I., Rinne, J., Misztal, P., Nemitz, E., Nilsson, D., Pryor, S., Gallagher, M. W., Vesala, T., Skiba, U., Brueggemann, N., Zechmeister-Boltenstern, S., Williams, J., O'Dowd, C., Facchini, M. C., de Leeuw, G., Flossman, A., Chaumerliac, N., and Erisman, J. W.: Atmospheric composition change: Ecosystems-Atmosphere interactions, ATMOSPHERIC ENVIRONMENT, 43, 5193–5267, https://doi.org/10.1016/j.atmosenv.2009.07.068, 2009.

Garland, J.: The dry deposition of sulphur dioxide to land and water surfaces, Proceedings of the Royal Society of London. A. Mathematical and Physical Sciences, 354, 245–268, 1977.

Garland, J. A. and Branson, J. R.: The deposition of sulphur dioxide to pine forest assessed by a radioactive tracer method, Tellus, 29, 445–454, https://doi.org/https://doi.org/10.1111/j.2153-3490.1977.tb00755.x, https://onlinelibrary.wiley.com/doi/abs/10.1111/j.2153-3490.1977.tb00755.x, 1977.

Guo, J., Wang, Y., Shen, X., Wang, Z., Lee, T., Wang, X., Li, P., Sun, M., Collett, J. L., Wang, W., and Wang, T.: Characterization of cloud water chemistry at Mount Tai, China: Seasonal variation, anthropogenic impact, and cloud processing, Atmospheric Environment, 60, 467–476, https://doi.org/https://doi.org/10.1016/j.atmosenv.2012.07.016, https://www.sciencedirect.com/science/article/pii/S1352231012006887, 2012.

Hoesly, R. M., Smith, S. J., Feng, L., Klimont, Z., Janssens-Maenhout, G., Pitkanen, T., Seibert, J. J., Vu, L., Andres, R. J., Bolt, R. M., et al.: Historical (1750-2014) anthropogenic emissions of reactive gases and aerosols from the Community Emission Data System (CEDS), Geoscientific Model Development, 11, 369–408, 2018.

Holland, D. M., Principe, P. P., and Sickles, J. E.: Trends in atmospheric sulfur and nitrogen species in the eastern United States for 1989-1995, Atmospheric Environment, 33, 37 – 49, https://doi.org/https://doi.org/10.1016/S1352-2310(98)00123-X, http://www.sciencedirect.com/science/article/pii/S135223109800123X, 1998.

Holtslag, A. A. M. and Bruin, H. A. R. D.: Applied Modeling of the Nighttime Surface Energy Balance over Land, Journal of Applied Meteorology and Climatology, 27, 689 – 704, https://doi.org/10.1175/1520-0450(1988)027<0689:AMOTNS>2.0.CO;2, https://journals.ametsoc.org/view/journals/apme/27/6/1520-0450_1988_027_0689_amotns_2_0_co_2.xml, 01 Jun. 1988.

Janssens-Maenhout, G., Crippa, M., Guizzardi, D., Dentener, F., Muntean, M., Pouliot, G., Keating, T., Zhang, Q., Kurokawa, J., Wankmueller, R., van der Gon, H. D., Kuenen, J. J. P., Klimont, Z., Frost, G., Darras, S., Koffi, B., and Li, M.: HTAPv2.2: a mosaic of regional and global emission grid maps for 2008 and 2010 to study hemispheric transport of air pollution, ATMOSPHERIC CHEMISTRY AND PHYSICS, 15, 11 411–11 432, https://doi.org/10.5194/acp-15-11411-2015, 2015.

Karset, I. H. H., Berntsen, T. K., Storelvmo, T., Alterskjær, K., Grini, A., Olivié, D., Kirkevåg, A., Seland, Ø., Iversen, T., and Schulz, M.: Strong impacts on aerosol indirect effects from historical oxidant changes, Atmospheric Chemistry and Physics, 18, 7669–7690, https://doi.org/10.5194/acp-18-7669-2018, https://acp.copernicus.org/articles/18/7669/2018/, 2018.

Kipling, Z., Stier, P., Schwarz, J. P., Perring, A. E., Spackman, J. R., Mann, G. W., Johnson, C. E., and Telford, P. J.: Constraints on aerosol processes in climate models from vertically-resolved aircraft observations of black carbon, ATMOSPHERIC CHEMISTRY AND PHYSICS, 13, 5969–5986, https://doi.org/10.5194/acp-13-5969-2013, 2013.

Kreidenweis, S. M., Walcek, C. J., Feingold, G., Gong, W., Jacobson, M. Z., Kim, C.-H., Liu, X., Penner, J. E., Nenes, A., and Seinfeld, J. H.: Modification of aerosol mass and size distribution due to aqueous-phase SO2 oxidation in clouds: Comparisons of several models, Journal of Geophysical Research: Atmospheres, 108, 2003.

Krotkov, N. A., McLinden, C. A., Li, C., Lamsal, L. N., Celarier, E. A., Marchenko, S. V., Swartz, W. H., Bucsela, E. J., Joiner, J., Duncan,
B. N., Boersma, K. F., Veefkind, J. P., Levelt, P. F., Fioletov, V. E., Dickerson, R. R., He, H., Lu, Z., and Streets, D. G.: Aura OMI
observations of regional SO2 and NO2 pollution changes from 2005 to 2015, Atmospheric Chemistry and Physics, 16, 4605–4629,
https://doi.org/10.5194/acp-16-4605-2016, https://acp.copernicus.org/articles/16/4605/2016/, 2016.

Kuhlbrodt, T., Jones, C. G., Sellar, A., Storkey, D., Blockley, E., Stringer, M., Hill, R., Graham, T., Ridley, J., Blaker, A., Calvert, D., Copsey,
D., Ellis, R., Hewitt, H., Hyder, P., Ineson, S., Mulcahy, J., Siahaan, A., and Walton, J.: The Low-Resolution Version of HadGEM3 GC3.1:
Development and Evaluation for Global Climate, JOURNAL OF ADVANCES IN MODELING EARTH SYSTEMS, 10, 2865–2888,
https://doi.org/10.1029/2018MS001370, 2018.

Lawrence, B. N., Bennett, V. L., Churchill, J., Juckes, M., Kershaw, P., Pascoe, S., Pepler, S., Pritchard, M., and Stephens, A.: Stor-
ing and manipulating environmental big data with JASMIN, in: 2013 IEEE International Conference on Big Data, pp. 68–75,
https://doi.org/10.1109/BigData.2013.6691556, 2013.

Lee, C., Martin, R. V., van Donkelaar, A., Lee, H., Dickerson, R. R., Hains, J. C., Krotkov, N., Richter, A., Vinnikov, K., and Schwab,
J. J.: SO2 emissions and lifetimes: Estimates from inverse modeling using in situ and global, space-based (SCIAMACHY and OMI)
observations, Journal of Geophysical Research: Atmospheres, 116, https://doi.org/https://doi.org/10.1029/2010JD014758, https://agupubs.
onlinelibrary.wiley.com/doi/abs/10.1029/2010JD014758, 2011.

Leibensperger, E. M., Mickley, L. J., Jacob, D. J., Chen, W.-T., Seinfeld, J. H., Nenes, A., Adams, P. J., Streets, D. G., Kumar, N., and
Rind, D.: Climatic effects of 1950ndash;2050 changes in US anthropogenic aerosols ndash; Part 1: Aerosol trends and radiative forcing,
Atmospheric Chemistry and Physics, 12, 3333–3348, https://doi.org/10.5194/acp-12-3333-2012, https://acp.copernicus.org/articles/12/
3333/2012/, 2012.

Levelt, P. F., Joiner, J., Tamminen, J., Veefkind, J. P., Bhartia, P. K., Stein Zweers, D. C., Duncan, B. N., Streets, D. G., Eskes, H., van der
A, R., McLinden, C., Fioletov, V., Carn, S., de Laat, J., DeLand, M., Marchenko, S., McPeters, R., Ziemke, J., Fu, D., Liu, X., Pickering,
K., Apituley, A., González Abad, G., Arola, A., Boersma, F., Chan Miller, C., Chance, K., de Graaf, M., Hakkarainen, J., Hassinen, S.,
Ialongo, I., Kleipool, Q., Krotkov, N., Li, C., Lamsal, L., Newman, P., Nowlan, C., Suleiman, R., Tilstra, L. G., Torres, O., Wang, H.,
and Wargan, K.: The Ozone Monitoring Instrument: overview of 14 years in space, Atmospheric Chemistry and Physics, 18, 5699–5745,
https://doi.org/10.5194/acp-18-5699-2018, https://acp.copernicus.org/articles/18/5699/2018/, 2018.

Li, J., Wang, X., Chen, J., Zhu, C., Li, W., Li, C., Liu, L., Xu, C., Wen, L., Xue, L., Wang, W., Ding, A., and Herrmann, H.: Chemical
composition and droplet size distribution of cloud at the summit of Mount Tai, China, Atmospheric Chemistry and Physics, 17, 9885–
9896, https://doi.org/10.5194/acp-17-9885-2017, https://acp.copernicus.org/articles/17/9885/2017/, 2017.

Li, J., Zhu, C., Chen, H., Fu, H., Xiao, H., Wang, X., Herrmann, H., and Chen, J.: A More Important Role for the Ozone-S (IV) Oxidation
Pathway Due to Decreasing Acidity in Clouds, Journal of Geophysical Research: Atmospheres, 125, e2020JD033 220, 2020.

Liu, F., Choi, S., Li, C., Fioletov, V. E., McLinden, C. A., Joiner, J., Krotkov, N. A., Bian, H., Janssens-Maenhout, G., Darmenov, A. S.,
and da Silva, A. M.: A new global anthropogenic SO2 emission inventory for the last decade: a mosaic of satellite-derived and bottom-up
emissions, Atmospheric Chemistry and Physics, 18, 16 571–16 586, https://doi.org/10.5194/acp-18-16571-2018, https://acp.copernicus.
org/articles/18/16571/2018/, 2018.

MACTEC-Engineering and Consulting, I. M.: Clean Air Status and Trends Network (CASTNET) 2004 Annual Report, Tech. rep., Prepared
for U. S. Environmental Protection Agency, Research Triangle Park, NC, USA, https://www3.epa.gov/castnet/docs/annual_report_2004.
pdf, 2005.

Mann, G. W., Carslaw, K. S., Spracklen, D. V., Ridley, D. A., Manktelow, P. T., Chipperfield, M. P., Pickering, S. J., and Johnson, C. E.: Description and evaluation of GLOMAP-mode: a modal global aerosol microphysics model for the UKCA composition-climate model, GEOSCIENTIFIC MODEL DEVELOPMENT, 3, 519–551, https://doi.org/10.5194/gmd-3-519-2010, 2010.

McHale, M. R., Ludtke, A. S., Wetherbee, G. A., Burns, D. A., Nilles, M. A., and Finkelstein, J. S.: Trends in precipitation chemistry across the U.S. 1985–2017: Quantifying the benefits from 30 years of Clean Air Act amendment regulation, Atmospheric Environment, 247, 118 219, https://doi.org/https://doi.org/10.1016/j.atmosenv.2021.118219, https://www.sciencedirect.com/science/article/pii/S1352231021000376, 2021.

Meagher, J. F., Bailey, E. M., and Luria, M.: The seasonal variation of the atmospheric SO2 to SO4 2??? conversion rate, Journal of Geophysical Research: Oceans, 88, 1525–1527, https://doi.org/https://doi.org/10.1029/JC088iC02p01525, https://agupubs.onlinelibrary.wiley.com/doi/abs/10.1029/JC088iC02p01525, 1983.

Met Office: Iris: A Python package for analysing and visualising meteorological and oceanographic data sets, Exeter, Devon, v1.2 edn., http://scitools.org.uk/, 2010 - 2013.

Met Office: Cartopy: a cartographic python library with a Matplotlib interface, Exeter, Devon, https://scitools.org.uk/cartopy, 2010 - 2015.

Meyers, T. P., Finkelstein, P., Clarke, J., Ellestad, T. G., and Sims, P. F.: A multilayer model for inferring dry deposition using standard meteorological measurements, Journal of Geophysical Research: Atmospheres, 103, 22 645–22 661, https://doi.org/https://doi.org/10.1029/98JD01564, https://agupubs.onlinelibrary.wiley.com/doi/abs/10.1029/98JD01564, 1998.

Monks, S. A., Arnold, S. R., Hollaway, M. J., Pope, R. J., Wilson, C., Feng, W., Emmerson, K. M., Kerridge, B. J., Latter, B. L., Miles, G. M., Siddans, R., and Chipperfield, M. P.: The TOMCAT global chemical transport model v1.6: description of chemical mechanism and model evaluation, Geoscientific Model Development, 10, 3025–3057, https://doi.org/10.5194/gmd-10-3025-2017, https://gmd.copernicus.org/articles/10/3025/2017/, 2017.

Mulcahy, J., Jones, C., Sellar, A., Johnson, B., Boutle, I., Jones, A., Andrews, T., Rumbold, S., Mollard, J., Bellouin, N., et al.: Improved aerosol processes and effective radiative forcing in HadGEM3 and UKESM1, Journal of Advances in Modeling Earth Systems, 10, 2786–2805, 2018.

Mulcahy, J. P., Johnson, C., Jones, C. G., Povey, A. C., Scott, C. E., Sellar, A., Turnock, S. T., Woodhouse, M. T., Abraham, N. L., Andrews, M. B., Bellouin, N., Browse, J., Carslaw, K. S., Dalvi, M., Folberth, G. A., Glover, M., Grosvenor, D. P., Hardacre, C., Hill, R., Johnson, B., Jones, A., Kipling, Z., Mann, G., Mollard, J., O'Connor, F. M., Palmiéri, J., Reddington, C., Rumbold, S. T., Richardson, M., Schutgens, N. A. J., Stier, P., Stringer, M., Tang, Y., Walton, J., Woodward, S., and Yool, A.: Description and evaluation of aerosol in UKESM1 and HadGEM3-GC3.1 CMIP6 historical simulations, Geoscientific Model Development, 13, 6383–6423, https://doi.org/10.5194/gmd-13-6383-2020, https://gmd.copernicus.org/articles/13/6383/2020/, 2020.

Murray, G. L., Kimball, K. D., Hill, L. B., Hislop, J. E., and Weathers, K. C.: Long-term trends in cloud and rain chemistry on Mount Washington, New Hampshire, Water, Air, & Soil Pollution, 224, 1653, 2013.

O'Connor, F. M., Johnson, C. E., Morgenstern, O., Abraham, N. L., Braesicke, P., Dalvi, M., Folberth, G. A., Sanderson, M. G., Telford, P. J., Voulgarakis, A., Young, P. J., Zeng, G., Collins, W. J., and Pyle, J. A.: Evaluation of the new UKCA climate-composition model - Part 2: The Troposphere, GEOSCIENTIFIC MODEL DEVELOPMENT, 7, 41–91, https://doi.org/10.5194/gmd-7-41-2014, 2014.

Paulot, F., Fan, S., and Horowitz, L. W.: Contrasting seasonal responses of sulfate aerosols to declining SO2 emissions in the Eastern U.S.: Implications for the efficacy of SO2 emission controls, Geophysical Research Letters, 44, 455–464, https://doi.org/https://doi.org/10.1002/2016GL070695, https://agupubs.onlinelibrary.wiley.com/doi/abs/10.1002/2016GL070695, 2017.

Payrissat, M. and Beilke, S.: Laboratory measurements of the uptake of sulphur dioxide by different European soils, Atmospheric Environment (1967), 9, 211 – 217, https://doi.org/https://doi.org/10.1016/0004-6981(75)90069-4, http://www.sciencedirect.com/science/article/pii/0004698175900694, 1975.

Pham, M., Muller, J., Brasseur, G., Granier, C., and Megie, G.: A 3D model study of the global sulphur cycle: Contributions of anthropogenic and biogenic sources, ATMOSPHERIC ENVIRONMENT, 30, 1815–1822, https://doi.org/10.1016/1352-2310(95)00390-8, Joint 8th CACGP/2nd IGAC Conference on Global Atmospheric Chemistry, FUJI, JAPAN, SEP 05-09, 1994, 1996.

Pope, R. J, H. C. L. C. and Chipperfield, M. P.: United Kingdom Earth System Model - Ozone Monitoring Instrument Total Column Sulphur Dioxide Comparisons, Tech. rep., Prepared for U. K. Met Office Hadley Centre, Met Office, Exeter, EX1 3PB, UK, https://digital.nmla.metoffice.gov.uk/io_697df5d9-e371-4492-82b9-12f9cfce64d7/, 2021.

Pope, R. J., Richards, N. A. D., Chipperfield, M. P., Moore, D. P., Monks, S. A., Arnold, S. R., Glatthor, N., Kiefer, M., Breider, T. J., Harrison, J. J., Remedios, J. J., Warneke, C., Roberts, J. M., Diskin, G. S., Huey, L. G., Wisthaler, A., Apel, E. C., Bernath, P. F., and Feng, W.: Intercomparison and evaluation of satellite peroxyacetyl nitrate observations in the upper troposphere–lower stratosphere, Atmospheric Chemistry and Physics, 16, 13 541–13 559, https://doi.org/10.5194/acp-16-13541-2016, https://acp.copernicus.org/articles/16/13541/2016/, 2016.

Revell, L. E., Kremser, S., Hartery, S., Harvey, M., Mulcahy, J. P., Williams, J., Morgenstern, O., McDonald, A. J., Varma, V., Bird, L., and Schuddeboom, A.: The sensitivity of Southern Ocean aerosols and cloud microphysics to sea spray and sulfate aerosol production in the HadGEM3-GA7.1 chemistry–climate model, Atmospheric Chemistry and Physics, 19, 15 447–15 466, https://doi.org/10.5194/acp-19-15447-2019, https://acp.copernicus.org/articles/19/15447/2019/, 2019.

Ridley, J. K., Blockley, E. W., Keen, A. B., Rae, J. G. L., West, A. E., and Schroeder, D.: The sea ice model component of HadGEM3-GC3.1, Geoscientific Model Development, 11, 713–723, 2018.

Sander, S., Friedl, R., Barker, J., Golden, D., Kurylo, M., Wine, P., Abbatt, J., Burkholder, J., Kolb, C., Moortgat, G., et al.: Chemical kinetics and photochemical data for use in atmospheric studies, evaluation number 14, JPL Publ., 02, 25, 334, 2003.

Saylor, R. D., Wolfe, G. M., Meyers, T. P., and Hicks, B. B.: A corrected formulation of the Multilayer Model (MLM) for inferring gaseous dry deposition to vegetated surfaces, Atmospheric Environment, 92, 141 – 145, https://doi.org/https://doi.org/10.1016/j.atmosenv.2014.03.056, http://www.sciencedirect.com/science/article/pii/S1352231014002416, 2014.

Schwab, J. J., Casson, P., Brandt, R., Husain, L., Dutkewicz, V., Wolfe, D., Demerjian, K. L., Civerolo, K. L., Rattigan, O. V., Felton, H. D., and Dukett, J. E.: Atmospheric Chemistry Measurements at Whiteface Mountain, NY: Cloud Water Chemistry, Precipitation Chemistry, and Particulate Matter, AEROSOL AND AIR QUALITY RESEARCH, 16, 841–854, https://doi.org/10.4209/aaqr.2015.05.0344, 2nd Atmospheric Chemistry and Physics at Mountain Sites Symposium, Steamboat Springs, CO, AUG 11-15, 2014, 2016.

Seland, Ø., Bentsen, M., Olivié, D., Toniazzo, T., Gjermundsen, A., Graff, L. S., Debernard, J. B., Gupta, A. K., He, Y.-C., Kirkevåg, A., et al.: Overview of the Norwegian Earth System Model (NorESM2) and key climate response of CMIP6 DECK, historical, and scenario simulations, Geoscientific Model Development, 13, 6165–6200, 2020.

Sellar, A. A., Jones, C. G., Mulcahy, J. P., Tang, Y., Yool, A., Wiltshire, A., O'Connor, F. M., Stringer, M., Hill, R., Palmieri, J., Woodward, S., de Mora, L., Kuhlbrodt, T., Rumbold, S. T., Kelley, I, D., Ellis, R., Johnson, C. E., Walton, J., Abraham, N. L., Andrews, M. B., Andrews, T., Archibald, A. T., Berthou, S., Burke, E., Blockley, E., Carslaw, K., Dalvi, M., Edwards, J., Folberth, G. A., Gedney, N., Griffiths, P. T., Harper, A. B., Hendry, M. A., Hewitt, A. J., Johnson, B., Jones, A., Jones, C. D., Keeble, J., Liddicoat, S., Morgenstern, O., Parker, R. J., Predoi, V., Robertson, E., Siahaan, A., Smith, R. S., Swaminathan, R., Woodhouse, M. T., Zeng, G., and Zerroukat, M.:

UKESM1: Description and Evaluation of the UK Earth System Model, JOURNAL OF ADVANCES IN MODELING EARTH SYSTEMS, 11, 4513–4558, https://doi.org/10.1029/2019MS001739, 2019.

Sickles, II, J. E. and Shadwick, D. S.: Seasonal and regional air quality and atmospheric deposition in the eastern United States, JOURNAL OF GEOPHYSICAL RESEARCH-ATMOSPHERES, 112, https://doi.org/10.1029/2006JD008356, 2007.

Sickles II, J. E. and Shadwick, D. S.: Air quality and atmospheric deposition in the eastern US: 20 years of change, Atmospheric Chemistry and Physics, 15, 173–197, https://doi.org/10.5194/acp-15-173-2015, https://acp.copernicus.org/articles/15/173/2015/, 2015.

Smith, F. and Jeffrey, G.: Airborne transport of sulphur dioxide from the U.K., Atmospheric Environment (1967), 9, 643 – 659, https://doi.org/https://doi.org/10.1016/0004-6981(75)90008-6, http://www.sciencedirect.com/science/article/pii/0004698175900086, 1975.

Smith, S.: Note bias in emissions data over western USA, Atmospheric Chemistry and Physics (2021), https://doi.org/https://doi.org/10.5194/acp-2021-238-CC1, 2021.

Storkey, D., Blaker, A. T., Mathiot, P., Megann, A., Aksenov, Y., Blockley, E. W., Calvert, D., Graham, T., Hewitt, H. T., Hyder, P., et al.: UK Global Ocean GO6 and GO7: A traceable hierarchy of model resolutions, Geoscientific Model Development, 11, 3187–3213, 2018.

Tan, J., Fu, J. S., Dentener, F., Sun, J., Emmons, L., Tilmes, S., Sudo, K., Flemming, J., Jonson, J. E., Gravel, S., Bian, H., Davila, Y., Henze, D. K., Lund, M. T., Kucsera, T., Takemura, T., and Keating, T.: Multi-model study of HTAP II on sulfur and nitrogen deposition, ATMOSPHERIC CHEMISTRY AND PHYSICS, 18, 6847–6866, https://doi.org/10.5194/acp-18-6847-2018, 2018.

Tang, Yongming; Rumbold, S. E. R. K. D. M. J. S. A. W. J. J. C.: MOHC UKESM1.0-LL model output prepared for CMIP6 CMIP historical CMIP historical, Version 20200818, Earth System Grid Federation, https://doi.org/10.22033/ESGF/CMIP6.6113, https://doi.org/10.22033/ESGF/CMIP6.6113, 2019.

Tang, Y. S., Braban, C. F., Dragosits, U., Simmons, I., Leaver, D., van Dijk, N., Poskitt, J., Thacker, S., Patel, M., Carter, H., Pereira, M. G., Keenan, P. O., Lawlor, A., Conolly, C., Vincent, K., Heal, M. R., and Sutton, M. A.: Acid gases and aerosol measurements in the UK (1999-2015): regional distributions and trends, ATMOSPHERIC CHEMISTRY AND PHYSICS, 18, 16 293–16 324, https://doi.org/10.5194/acp-18-16293-2018, 2018.

Torseth, K., Aas, W., Breivik, K., Fjaeraa, A. M., Fiebig, M., Hjellbrekke, A. G., Myhre, C. L., Solberg, S., and Yttri, K. E.: Introduction to the European Monitoring and Evaluation Programme (EMEP) and observed atmospheric composition change during 1972-2009, ATMOSPHERIC CHEMISTRY AND PHYSICS, 12, 5447–5481, https://doi.org/10.5194/acp-12-5447-2012, 2012.

Turnock, S. T., Mann, G. W., Woodhouse, M. T., Dalvi, M., O'Connor, F. M., Carslaw, K. S., and Spracklen, V, D.: The Impact of Changes in Cloud Water pH on Aerosol Radiative Forcing, GEOPHYSICAL RESEARCH LETTERS, 46, 4039–4048, https://doi.org/10.1029/2019GL082067, 2019.

Turnock, S. T., Spracklen, D. V., Carslaw, K. S., Mann, G. W., Woodhouse, M. T., Forster, P. M., Haywood, J., Johnson, C. E., Dalvi, M., Bellouin, N., and Sanchez-Lorenzo, A.: Modelled and observed changes in aerosols and surface solar radiation over Europe between 1960 and 2009, ATMOSPHERIC CHEMISTRY AND PHYSICS, 15, 9477–9500, https://doi.org/10.5194/acp-15-9477-2015, 2015.

Ukhov, A., Mostamandi, S., da Silva, A., Flemming, J., Alshehri, Y., Shevchenko, I., and Stenchikov, G.: Assessment of natural and anthropogenic aerosol air pollution in the Middle East using MERRA-2, CAMS data assimilation products, and high-resolution WRF-Chem model simulations, Atmospheric Chemistry and Physics, 20, 9281–9310, https://doi.org/10.5194/acp-20-9281-2020, https://acp.copernicus.org/articles/20/9281/2020/, 2020.

van Marle, M. J. E., Kloster, S., Magi, B. I., Marlon, J. R., Daniau, A.-L., Field, R. D., Arneth, A., Forrest, M., Hantson, S., Kehrwald, N. M., Knorr, W., Lasslop, G., Li, F., Mangeon, S., Yue, C., Kaiser, J. W., and van der Werf, G. R.: Historic global biomass burning emissions for

CMIP6 (BB4CMIP) based on merging satellite observations with proxies and fire models (1750–2015), Geoscientific Model Development, 10, 3329–3357, https://doi.org/10.5194/gmd-10-3329-2017, https://gmd.copernicus.org/articles/10/3329/2017/, 2017.

1130 VanCuren, R. T. and Gustin, M. S.: Identification of sources contributing to PM2.5 and ozone at elevated sites in the western U.S. by receptor analysis: Lassen Volcanic National Park, California, and Great Basin National Park, Nevada, Science of The Total Environment, 530-531, 505–518, https://doi.org/https://doi.org/10.1016/j.scitotenv.2015.03.091, https://www.sciencedirect.com/science/article/pii/S0048969715003666, 2015.

Vet, R., Artz, R. S., Carou, S., Shaw, M., Ro, C.-U., Aas, W., Baker, A., Bowersox, V. C., Dentener, F., Galy-Lacaux, C., Hou, A., Pienaar,
1135 J. J., Gillett, R., Cristina Forti, M., Gromov, S., Hara, H., Khodzher, T., Mahowald, N. M., Nickovic, S., Rao, P. S. P., and Reid, N. W.: A global assessment of precipitation chemistry and deposition of sulfur, nitrogen, sea salt, base cations, organic acids, acidity and pH, and phosphorus, ATMOSPHERIC ENVIRONMENT, 93, 3–100, https://doi.org/10.1016/j.atmosenv.2013.10.060, 2014.

Walters, D., Baran, A. J., Boutle, I., Brooks, M., Earnshaw, P., Edwards, J., Furtado, K., Hill, P., Lock, A., Manners, J., et al.: The Met Office Unified Model global atmosphere 7.0/7.1 and JULES global land 7.0 configurations, Geoscientific Model Development, 12, 1909–1963,
1140 2019.

Wang, Z., Xie, F., Sakurai, T., Ueda, H., Han, Z., Carmichael, G., Streets, D., Engardt, M., Holloway, T., Hayami, H., Kajino, M., Thongboonchoo, N., Bennet, C., Park, S., Fung, C., Chang, A., Sartelet, K., and Amann, M.: MICS-Asia II: Model inter-comparison and evaluation of acid deposition, Atmospheric Environment, 42, 3528–3542, https://doi.org/https://doi.org/10.1016/j.atmosenv.2007.12.071, https://www.sciencedirect.com/science/article/pii/S1352231008000101, mICS-ASIA II, 2008.

1145 Wesely, M.: Parameterization of surface resistances to gaseous dry deposition in regional-scale numerical-models, Atmospheric Environment, 23, 1293–1304, https://doi.org/10.1016/0004-6981(89)90153-4, 1989.

Williams, K. D., Copsey, D., Blockley, E. W., Bodas-Salcedo, A., Calvert, D., Comer, R., Davis, P., Graham, T., Hewitt, H. T., Hill, R., Hyder, P., Ineson, S., Johns, T. C., Keen, A. B., Lee, R. W., Megann, A., Milton, S. F., Rae, J. G. L., Roberts, M. J., Scaife, A. A., Schiemann, R., Storkey, D., Thorpe, L., Watterson, I. G., Walters, D. N., West, A., Wood, R. A., Woollings, T., and Xavier, P. K.: The Met Office Global
1150 Coupled Model 3.0 and 3.1 (GC3.0 and GC3.1) Configurations, JOURNAL OF ADVANCES IN MODELING EARTH SYSTEMS, 10, 357–380, https://doi.org/10.1002/2017MS001115, 2018.

Wu, T., Zhang, F., Zhang, J., Jie, W., Zhang, Y., Wu, F., Li, L., Yan, J., Liu, X., Lu, X., Tan, H., Zhang, L., Wang, J., and Hu, A.: Beijing Climate Center Earth System Model version 1 (BCC-ESM1): model description and evaluation of aerosol simulations, Geoscientific Model Development, 13, 977–1005, https://doi.org/10.5194/gmd-13-977-2020, 2020.

1155 Wys, J. N. D., Hill, A., and Robinson, E.: Assessment of the fate of Sulphur Dioxide from a point source, in: Sulfur in the Atmosphere, edited by HUSAR, R., LODGE, J., and MOORE, D., pp. 633 – 639, Pergamon, https://doi.org/https://doi.org/10.1016/B978-0-08-022932-4.50065-3, http://www.sciencedirect.com/science/article/pii/B9780080229324500653, 1978.

Yang, Y., Smith, S. J., Wang, H., Lou, S., and Rasch, P. J.: Impact of Anthropogenic Emission Injection Height Uncertainty on Global Sulfur Dioxide and Aerosol Distribution, JOURNAL OF GEOPHYSICAL RESEARCH-ATMOSPHERES, 124, 4812–4826,
1160 https://doi.org/10.1029/2018JD030001, 2019.

Yool, A., Palmi??ri, J., Jones, C. G., Sellar, A. A., de Mora, L., Kuhlbrodt, T., Popova, E. E., Mulcahy, J. P., Wiltshire, A., Rumbold, S. T., Stringer, M., Hill, R. S. R., Tang, Y., Walton, J., Blaker, A., Nurser, A. J. G., Coward, A. C., Hirschi, J., Woodward, S., Kelley, D. I., Ellis, R., and Rumbold-Jones, S.: Spin-up of UK Earth System Model 1 (UKESM1) for CMIP6, Journal of Advances in Modeling Earth Systems, 12, e2019MS001 933, https://doi.org/https://doi.org/10.1029/2019MS001933, https://agupubs.onlinelibrary.wiley.com/doi/abs/
1165 10.1029/2019MS001933, e2019MS001933 10.1029/2019MS001933, 2020.

Yool, A., Popova, E. E., and Anderson, T. R.: MEDUSA-2.0: an intermediate complexity biogeochemical model of the marine carbon cycle for climate change and ocean acidification studies, GEOSCIENTIFIC MODEL DEVELOPMENT, 6, 1767–1811, https://doi.org/10.5194/gmd-6-1767-2013, 2013.

Zhang, L., Brook, J., and Vet, R.: A revised parameterization for gaseous dry deposition in air-quality models, ATMOSPHERIC CHEMISTRY AND PHYSICS, 3, 2067–2082, https://doi.org/10.5194/acp-3-2067-2003, 2003.

Zhao, B., Jiang, J. H., Gu, Y., Diner, D., Worden, J., Liou, K.-N., Su, H., Xing, J., Garay, M., and Huang, L.: Decadal-scale trends in regional aerosol particle properties and their linkage to emission changes, Environmental Research Letters, 12, 054 021, https://doi.org/10.1088/1748-9326/aa6cb2, https://doi.org/10.1088/1748-9326/aa6cb2, 2017.

Zheng, B., Tong, D., Li, M., Liu, F., Hong, C., Geng, G., Li, H., Li, X., Peng, L., Qi, J., Yan, L., Zhang, Y., Zhao, H., Zheng, Y., He, K., and Zhang, Q.: Trends in China's anthropogenic emissions since 2010 as the consequence of clean air actions, Atmospheric Chemistry and Physics, 18, 14 095–14 111, https://doi.org/10.5194/acp-18-14095-2018, https://acp.copernicus.org/articles/18/14095/2018/, 2018.